Desalination and Water Treatment
www.deswater.com

doi: 10.5004/dwt.2022.28365

258 (2022) 241–260
May

Efficient elimination of Pb(II) ions from aqueous solutions using magnetic Fe_3O_4-nanoparticles/activated carbon derived from agricultural waste

Manal A. El-Sheeta[a,b], Mohamed E. Goher[b], Muhammad G. Abd El-Moghny[a], Mohamed S. El-Deab[a,*]

[a]*Department of Chemistry, Faculty of Science, Cairo University, Cairo, Egypt, Tel. +201012145268; emails: msaada@cu.edu.eg (M.S. El-Deab), manalabdelfatah92@yahoo.com (M.A. El-Sheeta), gmohamd@sci.cu.edu.eg (M.G. Abd El-Moghny)*
[b]*National Institute of Oceanography and Fisheries (NIOF), Cairo, Egypt, email: smgoher@yahoo.com*

Received 1 September 2021; Accepted 3 March 2022

ABSTRACT

Agricultural by-products are promising adsorbent materials for wastewater treatment, for example, removal of heavy metals. In this study activated carbons (AC) prepared from rice straw agricultural waste (treated with concentrated sulfuric acid) are used to remove lead ions (Pb^{2+}) from aqueous solutions in batch mode. The calcination of AC at 500°C for 1 h shows improved removal efficiency. Synthesized magnetite nanoparticles (Fe_3O_4-NPs) are loaded on AC with different ratios (Fe_3O_4/AC(1)), (Fe_3O_4/AC(2)) using co-precipitation method. The chemical structure, surface composition and morphology are characterized by scanning electron microscopy–energy-dispersive X-ray, X-ray diffraction, Fourier-transform infrared spectroscopy, Brunauer–Emmett–Teller and Raman spectroscopic analyses. The adsorption process depends on the initial metal ion concentration, temperature, solution pH, the adsorbent dose and contact time. Fe_3O_4/AC(2) has the highest adsorption capacity (68 mg g^{-1}) at 100 mg L^{-1} metal ion concentration, adsorbent dose of 1 g L^{-1}, room temperature (30°C ± 2°C), shaking speed = 200 rpm, contact time = 1 h and pH = 5. The thermodynamic studies show that the adsorption process fits Freundlich model (R^2 = 0.997) better than Langmuir and Temkin models. The adsorption/desorption kinetics of Pb^{2+} ions proceeds via pseudo-second-order kinetics. The temperature-dependent study (carried out in the range of 20°C–60°C) confirmed that the adsorption process was endothermic in nature.

Keywords: Rice straw; Magnetite nanoparticles; Active carbon; Calcination; Adsorption; Heavy metals; Isotherm; Kinetics

1. Introduction

Water is an important resource required for human life. Nowadays, water pollution has become a major environmental challenge and a hazard to the well-being of living organisms with various contaminants (mainly heavy metals). In nature, heavy metals are non-biodegradable, persistent, carcinogenic and toxic and are easily transported in the environment [1]. In living organisms, heavy metals are bio-accumulated (in what is called bio-magnification) through the food chain and their accumulation causes various diseases and malfunctions [2]. Naturally, heavy metals are present in low concentrations in the earth's crust, but they have become concentrated because of human activity that leads to environmental pollution [3]. Pb^{2+} ions are considered among the most toxic metals, it is a highly dangerous and long-standing environmental pollutant. Various industries, such as the production of batteries, glass, metal plating and finishing, printing and tanning, produce enormous amounts of waste water polluted with

* Corresponding author.

lead ions [4]. For pregnant women, poisoning with Pb(II) ions causes liver, kidney and hemoglobin formation damage, mental retardation, infertility and abnormalities. Moreover, anemia, headache, chills, diarrhea and toxicity may be directly or indirectly induced, contributing to dysfunction of the kidneys, reproductive organs, liver, brain and central nervous system [5].

Numerous procedures have been studied to remove lead ions from water such as precipitation, coagulation, ion exchange, electro-coagulation, filtration and adsorption [6]. Adsorption is one of the best methods for heavy metal ion removal because of it is a facile, high performance, cost-effective method in addition to its operational simplicity [7]. As adsorbents, activated carbon (AC) is recognized as an effective candidate due to its high porosity, large surface area, and high catalytic activity [8]. Researchers, in both developed and developing countries, have extensively studied the use of agricultural waste to extract heavy metals [9]. One of the most significant obstacles for commercial producers is the high cost of AC manufacturing [10]. The use of a simple method for the production of activated carbon can also greatly reduce production costs. So the abundance and availability of agricultural by-products make them excellent sources of raw materials for activated carbon preparation [11]. Activated carbon produced from agricultural wastes has been investigated for pollutant removal from aqueous solution like rice straw (RS) [12].

Rice is the second largest cereal crop in the world after maize, staple food by more than 50% of the world's population. In this context, rice straw (RS) has many structural and compositional features that enable its high absorptivity/adsorptivity of metals ions from aqueous solutions by the binding sites [13]. The chemical composition of RS predominantly contains cellulose (36%–40%), hemicellulose (15%–20%) and lignin (20%–23%) [14]. Rice husk (RH), RS and plastics are the primary solid waste in rice production [15], the burning of rice straw is a common practice after harvest which creates air pollution because of large amount of N_2O, SO_2, CH_4 and smoke are generated [16]. So it is crucial to reuse RS as a sorbent candidate.

Many of the activated carbons were generated through a two-steps, carbonization process then activation (chemical activation or physical activation). In physical activation, the precursor needs high temperatures (800°C–1,100°C) in the presence of oxidizing agents such as air, steam, CO_2 or a mixture of them [17]. Whereas, chemical activation takes place at much lower temperatures (400°C–600°C) [17]. The precursor is combined with a concentrated solution of an active agent which acts as dehydrating agent and oxidant [18], for example, H_3PO_4, $ZnCl_2$, H_2SO_4, and KOH allowing the formation of porous structures in the material [18]. The two steps are carried out simultaneously in the chemical activation process [19]. Chemical activation provides many advantages as it is carried out in a single stage, integrating carbonization and activation at lower temperatures and thereby contributing to the creation of a better porous structure [20]. Activation with acid breaks the covalent connection between components of lignocellulose, hemicellulose hydrolysis and lignin depolymerization, thus, increasing cellulose exposure, which further improves the adsorption properties of RS [21]. If we compare the surface area of the ACs prepared with H_2SO_4, H_3PO_4, $ZnCl_2$, the surface area of the AC treated with sulfuric acid was found to be the highest. The basic criteria for an effective adsorbent are high surface area and pore structure and these parameters are added by chemical activating agents such as H_2SO_4 [22]. This is due to the degradation of cellulosic content in plant materials and the aromatization of the carbon skeleton after H_2SO_4 treatment [23]. A review of literature on using rice residual waste for heavy metal removal is carried out by various researchers. Singha and Das [24] investigated the adsorption of Cu(II) by rice straw and rice bran with maximal adsorption capacities of 18.4 and 21.0 mg g^{-1}, respectively. Khan et al. [25] investigated the adsorption of hexavalent chromium [Cr(VI)] from aqueous solution by acidically produced rice husk carbon (APRHC). Also the removal of Cr(VI) from water by carbon produced from the burning of rice straw is investigated by Hsu et al. [26]. The rapid adsorption of toxic Hg(II) from the liquid phase onto rice straw activated carbon (RSAC) manufactured employing microwave-assisted H_2SO_4 activation was thoroughly researched and explained by Mashhadi et al. [11]. Rocha et al. [27] modified rice straw by HNO_3 and NaOH and use it to remove Cu(II), Zn(II), Cd(II) and Hg(II) ions from aqueous solutions with maximum adsorptions at pH 5 and time less than 1.5 h.

In this paper rice straw treated with hot concentrated H_2SO_4 which acts as a strong dehydrating and oxidizing agent due to its ability to lose an oxygen atom to form H_2SO_3, which quickly decomposes to SO_2 and H_2O. This will lead to carbonaceous material loaded with function groups such as –OH and –COOH on the surface [28]. Recent years have seen a greater interest in the use of nanoparticles as adsorbents in water treatment. Nanotechnology is the best possible method of treating both persistent and emerging contaminants [29]. It deals with nano-scale materials which often possess the novel size-dependent properties that differ from their larger counterparts. The small size and high surface area to volume ratio make nanomaterials detect highly sensitive contaminants [30].

Iron oxide is an ideal adsorbent since it has a high surface area to volume ratio. Excellent magnetic properties, great biocompatibility, ease of separation using external magnetic field, reusability, comparatively low cost and its surface can be modified. Also, because of variable oxidation states, it may coordinate with other components [22]. The use of magnetic nanoparticles in extracting heavy metals and dangerous materials from water has recently been studied by several researchers, demonstrating the efficiency of these materials. Among the magnetic materials, magnetite nanoparticles (Fe_3O_4-MNPs) are extremely effective and in recent years they have gained considerable attention and experimental emphasis [22]. These particles can be synthesized by various methods like sol-gel, chemical co-precipitation and hydrothermal methods. These nanoparticles have unique properties and a range of positive features in terms of their use, such as low cost and toxicity, strong magnetism, durability and biocompatibility, fast separation of water and their capacity for industrial applications [31]. It may be less efficient to use activated carbon alone, but when combined with a magnifying material, it may be

more effective in purification processes. Magnetic separation is a fast and efficient method of metal ion separation [32]. Another benefit is that the loaded adsorbents can be conveniently isolated by magnet instead of centrifugation from the aqueous solution, thereby saving energy [22]. This combination has transformed the rice straw waste into useful magnetic activated carbon sorbents for removing toxic ions from water. For the removal of Pb^{2+} ions from aqueous environments, several researchers have employed activated carbon as an adsorbent such as Ghasemi et al. [33] who synthesized Fig sawdust activated carbon (FSAC) by chemical activation with H_3PO_4 to remove Pb(II) ions from aqueous solution. The removal efficiency of Pb(II) ions via adsorption was reported to be highest (95.8%) at pH 4. Mouni et al. [5] also removed Pb(II) from dilute aqueous solution by AC produced by chemical activation of Apricot stone with sulphuric acid with maximum adsorption capacity of 21.38 mg g^{-1}. Shekinah et al. [34] removed Pb(II) ions from aqueous solution using activated carbon from aquatic weed, *Eichhornia* with adsorption capacity 16.61 mg g^{-1}. The possibility of using raw rice straw to remove Pb(II) from water by biosorption was explored by Amer et al. [35]. At a pH of 5.5 and a dose of 4 g L^{-1} at an initial Pb^{2+} concentration of 40 mg L^{-1} maximum removal of 94% was achieved. Using the Langmuir isotherm, RS had a maximum adsorption capacity of 42.55 mg g^{-1}. In this section, we will discuss recent research findings on the use of active carbon supported with magnetite nanomaterials to remove heavy metals. Zarandi et al. [36] produced magnetic nanoparticles (Fe_3O_4) which immobilized on activated carbon (AC) and used as an effective adsorbent for Cu(II) ions removal from aqueous solution. Fatehi et al. [37] studied the ability of produced magnetic nanoparticles supported on activated carbon (AC-MNPs) to remove Pb(II) and Cr(VI) ions from single and binary component aqueous solutions in the presence of salinity in order to manufacture an efficient and low-cost adsorbent. Khandanlou et al. [38] produced successfully small sized magnetite iron oxide nanoparticles (Fe_3O_4-NPs) in the absence of heat treatment on the surface of rice straw using the rapid precipitation method. Kakavandi et al. [39] synthesized the magnetic Fe_3O_4 nanoparticles using chemical co-precipitation and magnetized powder activated carbon (PAC). (Fe_3O_4@C) was used as an adsorbent for lead ions (Pb^{2+}) from aqueous solution with maximum monolayer adsorption capacity of 71.42 mg g^{-1} at 50°C. Nethaji et al. [40] used activated carbon made from corn cob biomass and magnetized by magnetite nanoparticles (MCCAC) to achieve the adsorption of Cr(VI) from aqueous solution with maximum mono layer adsorption capacity of 57.37 mg g^{-1}. Luo et al. [41] synthesized magnetic Fe_3O_4-loaded porous carbons composite (MRH) from rice husk for removal of arsenate As(V) with maximum absorption quantity (q_m) of 4.33 mg g^{-1}. The adsorption of Cu(II) and Pb(II) ions onto magnetic-plum stone activated carbon (m-PSAC) is investigated by Parlayıcı and Pehlivan [32]. The maximum adsorption capacities of Cu(II) and Pb(II) ions calculated by the Langmuir model were 48.31 and 80.65 mg g^{-1}, respectively.

In this work, the activated carbon was prepared from lignocellulosic agricultural by-product, rice straw by simple chemical activation without using inert gas or high temperature. The activated carbon was modified by loading its surface with the magnetite nanoparticles using a co-precipitation method in one step. This would make the water treatment process eco-friendly, effective and economically more attractive. This study also has another way for modification of the (AC) by thermal treatment (calcination at 500°C for 1 h in a muffle furnace in air) and compared with the synthesized magnetic rice straw activated carbon (Fe_3O_4/AC). All adsorbents used for the adsorption of lead ions (Pb^{2+}) from aqueous solution. Characterization and batch-type removal experiments were carried under various operating process conditions.

2. Experimental

2.1. Chemicals

All the chemicals used were of analytical grade (Sigma-Aldrich, Germany). Stock solution of 1,000 mg L^{-1} concentration of $Pb(NO_3)_2$ was prepared in double distilled water acidified with nitric acid to prevent hydrolysis. All the working solutions were made by proper dilution of the stock solution. The pH of each working solution was adjusted to the required value by using 0.1 M NaOH or 0.1 M HCl and measured using an electronic pH meter (WTW inoLab pH 730, Germany). The concentrations of the heavy metals in the solutions were determined by GBC Atomic Absorption Reader (Model SavantAA AAS with GF 5000 Graphite Furnace).

2.2. Preparation of activated carbon from rice straw (chemical activation) [28]

Rice straw (RS) was cut into small pieces and washed with water then allowed drying at room temperature. The above dried rice straw was crushed into fine powder in a steel mill. Crushed powder was boiled in distilled water for 2 h to remove dust and other soluble materials and dried in hot air oven at 60°C for 24 h. The washed grounded material was sieved in the size range of 250 μm; 200 g of it was added to 1,000 mL of 13 M sulfuric acid. The mixture was heated at 180°C for 3 h using a magnetic hot plate stirrer. The resulting black mixture was cooled and then filtered under vacuum using a Buchner funnel; it was washed several times with distilled water to a neutral pH and dried at 105°C in a hot air oven for 24 h. The dried activated carbon (AC) was crushed in a mortar and sieved in the size range of 63 μm and stored in a desiccator for further use.

2.3. Preparation of (Fe_3O_4/AC) nanoparticles

The co-precipitation method was used to prepare two distinct ratios of (Fe_3O_4/AC) NPs as reported by [22] with some modification. 2.5 g of AC for ((Fe_3O_4/AC(1)) and 1.25 g of AC for (Fe_3O_4/AC(2)) were dispersed in 250 mL solution of 28 mM $FeCl_3{\cdot}6H_2O$ and 14 mM of $FeSO_4{\cdot}7H_2O$ with vigorous stirring at 700 rpm at 70°C–80°C. 100 mL of NaOH (5 M) solution was added drop wise into the above mixture to precipitate the hydrated iron oxide under vigorous stirring at 80°C until pH reached 10–11. The suspension

was further stirred for 1h on a magnetic stirrer at 80°C. Next, it was aged at room temperature for 24 h. The (Fe_3O_4/AC) NPs were separated by a magnet and washed continuously with distilled water and ethanol up to neutral pH then dried in a hot air oven at 80°C for 12 h. After drying, the nanoparticles were crushed in a mortar and placed in airtight plastic containers for further use.

2.4. Calcination of the active carbon

The activated carbon (AC) prepared from RS by concentrated sulfuric acid was further modified by thermal treatment at 500°C for 1 h in a muffle furnace without inert gas. After that the calcined AC was cooled and placed in airtight plastic containers for further use. This method resulted in a substantial increase in the porosity of the material so surface area, pore volume and pore size increased.

2.5. Characterizations

2.5.1. Surface area analysis

The Brunauer–Emmett–Teller (BET) surface area, pore volume and pore diameter were determined by Barrett–Joyner–Halenda desorption method in N_2 atmosphere at 77 K using Quantachrome Nova 3200 instrument (Boynton Beach, FL, USA).The samples before measurement were degassed at 200°C for 24 h to remove moisture.

2.5.2. Fourier-transform infrared analysis

Fourier-transform infrared (FTIR) spectra of the samples were recorded using Fourier-transform infrared spectrometer (FTIR, 4100 JASCO, Japan) in the wavelength range of 4,000–400 cm^{-1} at a resolution of 4 cm^{-1}.

2.5.3. X-ray diffraction analysis

The crystalline structure of the nanoparticles and the amorphous nature of active carbon were checked using a Bruker AXS-D8 Advance X-ray diffraction (XRD) spectrometer (Karlsruhe, Germany). The scan was collected in the 2θ range from 4° to 80° with a step size of 0.02° and scan step time of 0.6 s using Cu-Kα (K = 1.5406 Å) operated at 40 kV and current of 40 mA.

2.5.4. Field-emission scanning electron microscopy and energy-dispersive X-ray analysis

The elemental analysis and morphology of surface of Fe_3O_4/AC NPs were determined via Field-emission scanning electron microscopic (FE-SEM) technique (Zeiss Sigma 300 VP) coupled with energy-dispersive X-ray (EDX) Oxford X-MAX.

2.5.5. Raman spectroscopic analysis

Due to its sensitivity to various carbon structures, Raman spectroscopy is specifically used to classify carbon-based materials. Raman spectra were achieved in SENTERRA dispersive Raman microscope (Bruker, Billerica, MA, USA).

3. Batch adsorption experiments

Batch adsorption experiments were performed to determine the elimination of (Pb^{2+}) from aqueous solution. In each experiment, 25 mL of Pb^{2+} ions solution of known initial concentration (ranging from 10 to 100 mg L^{-1}) was treated with a specified known amount (by wt.) of adsorbents (0.25–4 g L^{-1}) and at known pH. The solution pH was adjusted to the desired value by adding 0.1 M HCl or 0.1 M NaOH. Then, shaker flasks were agitated in a mechanical shaker at a constant speed of 200 rpm at room temperature (30°C ± 2°C) for a prescribed time to attain the equilibrium. Then the solutions were filtered and the final concentrations of metal ions were analyzed by using GBC atomic absorption reader (Model SavantAA AAS with GF 5000 Graphite Furnace). The effects of initial concentration of Pb^{2+} ions (10–100 mg L^{-1}), contact time (2–120 min), solution pH (3–5) and adsorbent dose (0.25–4.0 g L^{-1}) were studied. Blank solutions were treated similarly (without adsorbent) and the concentration at the end of each operation was taken as the initial one. The percent metal removal (R%) was calculated using Eq. (1):

$$R(\%) = \frac{C_i - C_e}{C_i} \times 100 \tag{1}$$

where C_i and C_e represented initial and equilibrium concentrations of metals in the solution respectively. The adsorption capacity (q_e) at equilibrium time was calculated using Eq. (2):

$$q_e(\text{mg/g}) = \frac{(C_i - C_e) \times v}{m} \tag{2}$$

where v is the volume of metal ion solution (L) and m is the mass of the adsorbent (g).

4. Results and discussion

4.1. Characterizations of adsorbents

The data in Table 1 indicates that the surface area and pore volume increased when magnetite nanoparticles loaded on AC obtained from rice straw Fe_3O_4/AC(1,2) and also when AC calcined at 500°C for 1 h.

The FTIR technique is an important tool for the identification of the characteristic functional groups involved in metal ion adsorption. Adsorbents have the ability to bind with metal ions with different kinds of chemical groups such as carboxyl, hydroxyl, ester, aldehyde, ketone etc. Their metal uptake affinity depends on variables such as the number of sites, their availability, chemical structure, affinity between binding sites and metal ions, etc [42]. FTIR spectra of AC, CAC and Fe_3O_4/AC(1) and (2) are shown in Fig. 1. Activation of RS with sulfuric acid indicated the presence of the acidic groups on the active carbon surface, which increases metal adsorption.

The FTIR spectrum of AC shows a broad peak at 3,397.96 cm^{-1} is due to –OH stretching of the H-bond which confirms the presence of the hydroxyl group [43]. Bands at 2,923.56 and 2,857.02 cm^{-1} are ascribed to the asymmetric

Table 1
Surface area, total pore volume and average pore diameter of AC, CAC and Fe_3O_4/AC(1,2)

Adsorbent	BET surface area ($m^2\ g^{-1}$)	Average pore diameter (nm)	Total pore volume ($cm^3\ g^{-1}$)
AC	22.75	3.4	0.04
CAC	204.69	10.3	0.28
Fe_3O_4/AC(1)	38.03	15.3	0.16
Fe_3O_4/AC(2)	109.89	10.5	0.54

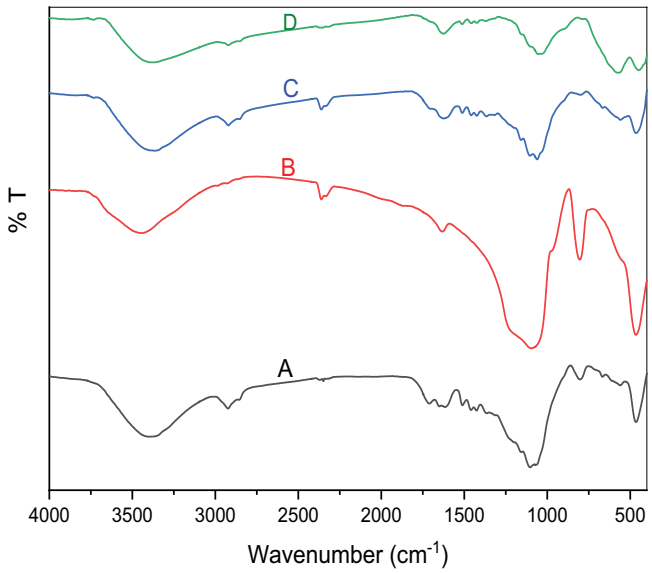

Fig. 1. FTIR spectra of: (A) AC, (B) CAC, (C) Fe_3O_4/AC(1), and (D) Fe_3O_4/AC(2).

and symmetric C–H stretching vibration models of aliphatic molecules, respectively [44]. The small band at 2,334.41 cm^{-1} is corresponding to the carboxyl group [43]. The smaller shoulder peaks at 1,710.55 and 1,616.06 cm^{-1} are attributed to unionized C=O stretching of carboxylic acid and C=O stretching of carboxylic group with intermolecular hydrogen bond, respectively [21]. The peaks at 1,510.9 and 1,458.89 cm^{-1} are indicative of the aromatic C=C stretching vibration in lignin aromatic groups [45]. The strong peak at 1,103 cm^{-1} is attributed to C–O stretching vibration and O–H bending modes of alcoholic, phenolic, and carboxylic groups. The C–H out-of-plane bending vibrations in aromatic structures cause the band at 802.242 cm^{-1} [46]. So, it can be concluded that there exists hydroxyl, carbonyl and carboxyl groups on the AC surface. After calcination of AC small peaks at 3,900 and 3,840 cm^{-1} may be ascribed to isolated OH groups and the strong broad peak centered at 3,443.2 cm^{-1} can be assigned to O–H stretching vibration of hydroxyl functional groups [46]. After calcination great changes occurred to AC chemical composition and the peaks shifted as compared to AC. At high temperature silica content increased and this confirmed by the strong peaks at 1,097.3 and 804.2 cm^{-1} which play a vital role in the adsorbent development [47], the peak at 1,097.3 cm^{-1} is very strong due to asymmetric stretching of Si–O and Si–O–Si stretching in silica at 465.7 cm^{-1}. The weak band of aliphatic groups stretching vibration at 2,930.3 cm^{-1} its intensity was lower than the spectrum of AC, leading to the decrease in aliphaticity in the activated carbon by increasing temperature. Bands at 1,510.9 and 1,458.89 cm^{-1} which are indicative of the aromatic C=C stretching vibration in lignin aromatic groups disappeared because of the removal of most of the lignin. Residual lignin ascribed at the smaller shoulder peak at 1,632.5 cm^{-1}. At the same time two bands of carboxyl groups appeared at 2,360.4 and 2,334.4 cm^{-1}. On the other hand, in Fe_3O_4/AC(1) and (2), the presence of Fe_3O_4-NPs on the surface of AC is evidenced by the new adsorption bands observed at 666.3 and 558.3 cm^{-1} for Fe_3O_4/AC(1) and at 787.8, 574.7 cm^{-1} for Fe_3O_4/AC(2), respectively, which corresponds to Fe–O stretching in Fe_3O_4 [36,41]. Absorption peaks at 3,365.2 and 3,370.9 cm^{-1} in Fe_3O_4/AC(1) and Fe_3O_4/AC(2), respectively, are characterized by OH groups, indicating the presence of AC [38]. The shifting of those peaks and other peaks of the function groups of AC is due to the binding of Fe_3O_4-NPs with AC and confirm (Fe_3O_4/AC) preparation.

The comparison of XRD patterns of the four samples (Fig. 2) indicates that the iron oxide nanoparticles in Fe_3O_4/AC samples are crystalline in nature and have the cubic structure of magnetite. The XRD pattern (Fig. 2C) of Fe_3O_4/AC(1) shows four characteristic diffraction peaks (with corresponding Miller indices) at 2θ of 33.14° (220), 35.55° (311), 54.15° (422) and 62.41° (440) respectively. Also (Fig. 2D) of Fe_3O_4/AC(2) shows four characteristic diffraction peaks (with corresponding Miller indices) at 2θ of 35.69° (311), 43.25° (400), 57.22° (511) and 62.86° (440) respectively. These observations were in line with previous research [22,31,41,44,48–52]. (Fig. 2A and B) of the activated carbon didn't show any specific peak confirming that the AC is amorphous in nature which is a beneficial property for AC [3,53] but a broad diffraction hump was observed at 2θ range of 23° which is attributed to AC from rice straw. Also the presence of this hump in Fe_3O_4/AC(1,2) samples confirms the existence of Fe_3O_4-NPs on the AC surface.

FE-SEM micrographs as shown in Fig. 3 were used to study surface morphologies and texture of the four samples. The FE-SEM image reveals that the AC has a rough surface and pores due to the dehydrating effect of the activating agent (Concentrated H_2SO_4). As indicated in (Fig. 3A and B) the surface of the calcined AC became rougher and had a higher porosity which consecutively leads to a higher surface area as proved in BET analysis. Some of the AC has a tubular shape as confirmed by XRD analysis and porous structure (Fig. 3C and D) and Fe_3O_4-NPs distributed inside AC and on its surface. This viewed the higher surface

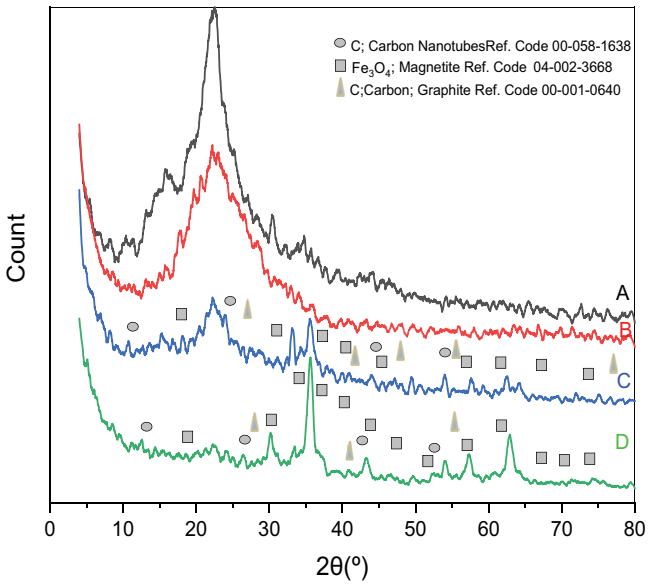

Fig. 2. XRD patterns of: (A) AC, (B) CAC, (C) Fe_3O_4/AC(1), and (D) Fe_3O_4/AC(2).

area of Fe_3O_4/AC(2) than Fe_3O_4/AC(1) because it had more Fe_3O_4-NPs agglomerated and attached to each other making the surface rough and coarse. EDX gives the elemental composition of the four adsorbents as shown in Fig. 4.

As can be seen in the EDX spectra of AC samples (Fig. 4A and B), they contain carbon, Oxygen and silicon which originated from silica present in rice straw. Fig. 4C and D show the presence of Fe along with C and O in Fe_3O_4/AC(1) and (2) samples, which confirmed the infusion of Fe_3O_4-NPs on the AC surface. This analysis also illustrated that the weight fraction of carbon is 50.24% and iron content is only 8.88% in Fe_3O_4/AC(1), indicating that the activated carbon content was significantly higher than Fe_3O_4 NPs. On the other hand, the weight fraction of carbon is only 28.15% but iron content is 32.86% in Fe_3O_4/AC(2), confirming that Fe_3O_4 NPs were more than AC. Moreover, the EDX spectrum of Fe_3O_4/AC(1) and (2) samples showed an additional peak which was assigned to Na that might have originated during Fe_3O_4 NPs preparation.

Raman spectroscopy is primarily applied to the characterization of carbon-based materials. The G band refers to the presence of sp^2 carbon in graphite-like structures and the D band is referred to as disorders/defects in graphitic

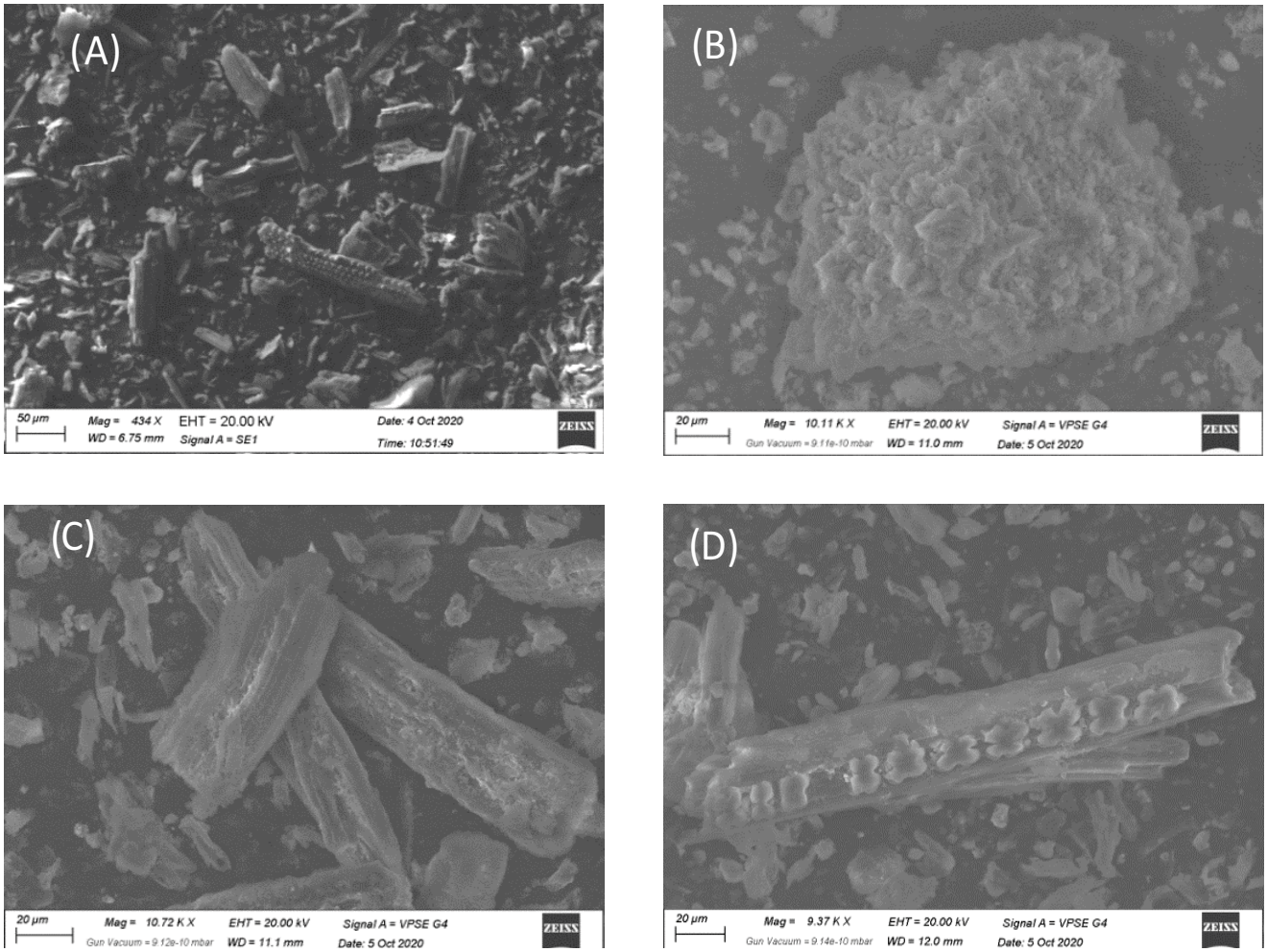

Fig. 3. FE-SEM images of: (A) AC, (B) CAC, (C) Fe_3O_4/AC(1), and (D) Fe_3O_4/AC(2).

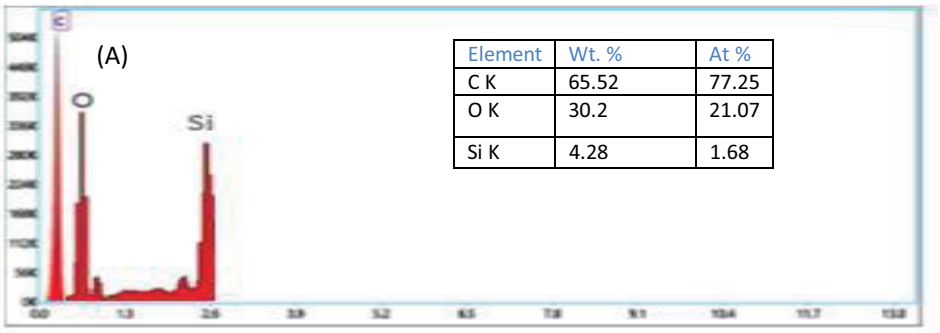

Element	Wt. %	At %
C K	65.52	77.25
O K	30.2	21.07
Si K	4.28	1.68

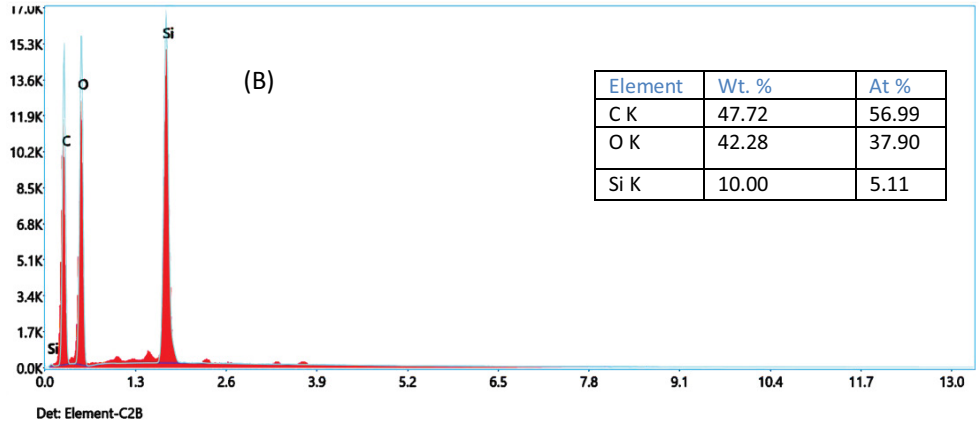

Element	Wt. %	At %
C K	47.72	56.99
O K	42.28	37.90
Si K	10.00	5.11

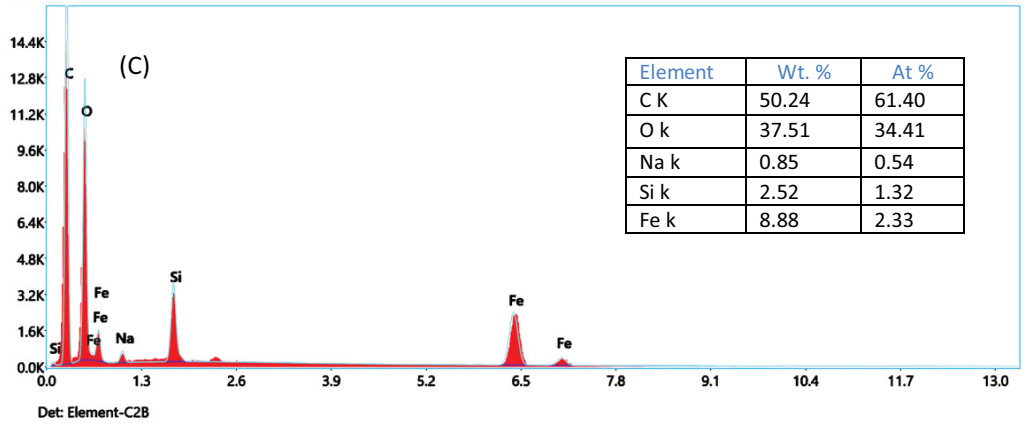

Element	Wt. %	At %
C K	50.24	61.40
O k	37.51	34.41
Na k	0.85	0.54
Si k	2.52	1.32
Fe k	8.88	2.33

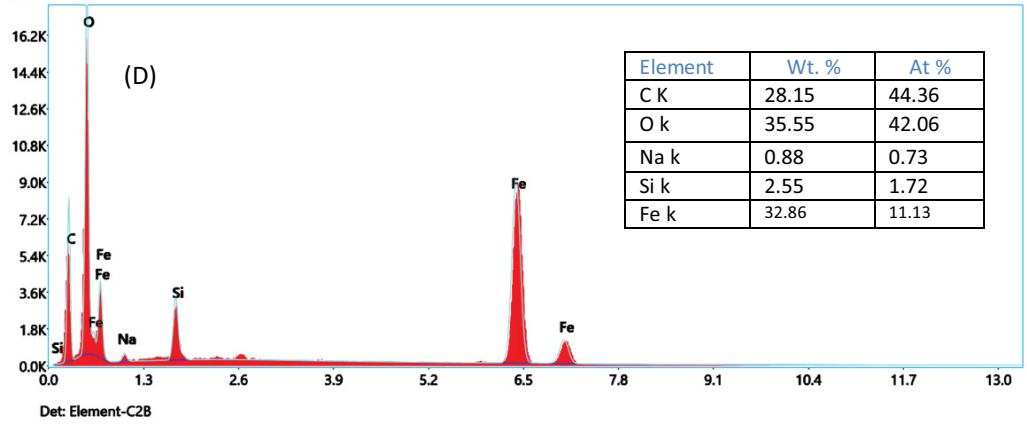

Element	Wt. %	At %
C K	28.15	44.36
O k	35.55	42.06
Na k	0.88	0.73
Si k	2.55	1.72
Fe k	32.86	11.13

Fig. 4. EDX spectra of: (A) AC, (B) CAC, (C) Fe_3O_4/AC(1), and (D) Fe_3O_4/AC(2).

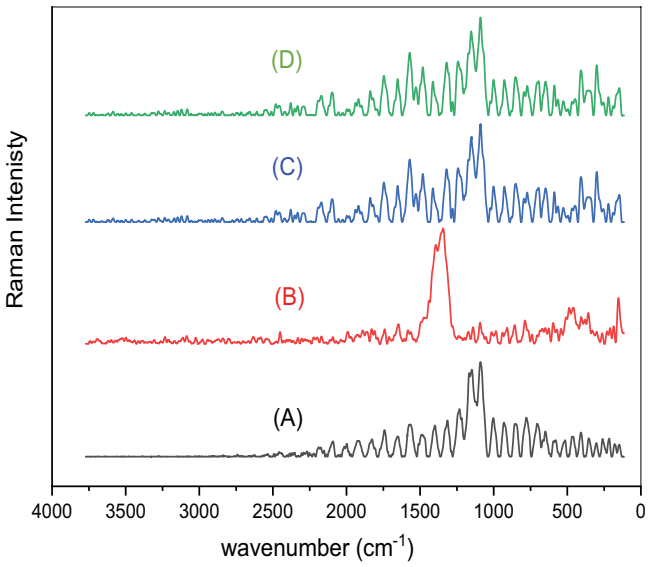

Fig. 5. Raman spectra of: (A) AC, (B) CAC, (C) Fe_3O_4/AC(1), and (D) Fe_3O_4/AC(2).

Table 2
G and D bands and their comparative intensity ratios (I_D/I_G) of the four samples

Adsorbent	D band (cm^{-1})	G band (cm^{-1})	I_D/I_G
AC	1,089.99	1,148.30	1.087
CAC	1,343.22	1,393.49	1.166
Fe_3O_4/AC(1)	1,089.11	1,150.20	1.113
Fe_3O_4/AC(2)	1,089.73	1,152.87	1.165

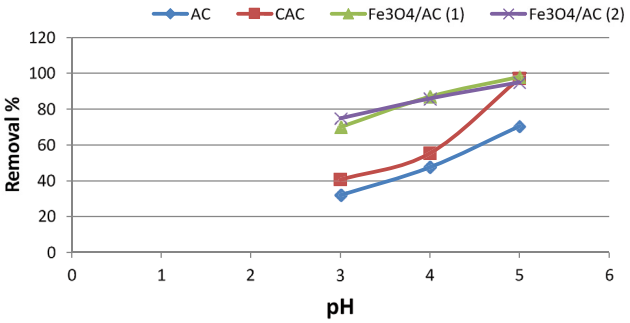

Fig. 6. Effect of pH on the removal of Pb^{2+} by the different adsorbents at initial concentration of 10 mg L^{-1}, 1 h, dose (2 g L^{-1}) of (AC, CAC and Fe_3O_4/AC(1)) and (1 g L^{-1}) of Fe_3O_4/AC(2), at room temperature (30°C ± 2°C) and shaking speed = 200 rpm.

structures. The Raman spectrum of the AC exhibits G, and D bands, at 1,148.30 and 1,089.99 cm^{-1}, respectively. As shown in Fig. 5 shifting occurred to (G, D) bands values in CAC and also in Fe_3O_4/AC(1) and (2).

In the graphitic structure of the activated carbon, the intensity ratio (I_D/I_G) of the D and G bands is the ratio of sp^3 hybridized carbon atoms (amorphous/disordered carbon) to sp^2-bonded carbon atoms (graphitic carbon) which is attributed to defects; the higher the intensity ratio, the higher degree of graphitic defects. A greater I_D/I_G quantity demonstrates a higher surface area and a higher amount of covalent reactions exist on the adsorbent surface [1,54]. It was calculated as indicated in (Table 2); Fe_3O_4/AC(2) and CAC have the highest I_D/I_G then Fe_3O_4/AC(1) and AC has the lowest ratios.

4.2. Batch studies

4.2.1. Effect of pH

The solution pH has an important impact on the adsorption of the metal ions by the adsorbents because its effect on the solubility of adsorbates, chemical status of the functional groups responsible for adsorption and the degree of ionization of the adsorbate during reaction [33]. Maximum adsorption has been found to occur at a particular pH value [55]. To determine the optimum adsorption pH, Fig. 6 shows the influence of pH on the adsorption of Pb^{2+}. While screening the pH values, all the other process variables such as initial metal ion concentration (10 mg L^{-1}), (AC, CAC and Fe_3O_4/AC(1)) dose (2 g L^{-1}) and Fe_3O_4/AC(2) dose (1 g L^{-1}), at room temperature (30°C ± 2°C), shaking speed (200 rpm) and contact time (1 h) were maintained constant.

Fig. 6 shows the maximum removal efficiency percentage of Pb^{2+} from aqueous solution by using AC, CAC, Fe_3O_4/AC(1) and Fe_3O_4/AC(2) was found to be 70.6%, 97%, 98% and 95%, respectively, at solution pH 5. The charge of active sites accessible on the surface of an adsorbent, which is usually influenced by the pH of the solution, affects the adsorption of lead ions onto the surface of an adsorbent. This is due to the fact that the H^+ is a strong competing adsorbate, and the chemical speciation of metal ions as the pH of the solution changes. At low pH, lower adsorption of metal ions onto the adsorbents due to the presence of excess H^+ ions competing with the metal ions for the active sites. The abundance of hydronium ions (H_3O^+) in the solution, causing competition for adsorption onto adsorbent surface between hydronium ions and Pb^{2+} ions (Lead ions is present as Pb^{2+} and Pb $(OH)^+$ at lower pH), lowering the overall adsorption efficiency of these metal ions at lower pH. On the other hand, at higher pH levels the functional groups present on the surface of nanoparticles, such as carboxylic acid, hydroxyls, and phenol, are deprotonated, resulting in negative sites on the adsorbent surface. As a result of the electrostatic interaction between these negatively charged adsorption sites and positively charged Pb^{2+} ions, the adsorption is increased [56]. As a result, the formation of hydroxide precipitation ($Pb(OH)_2$) at pH higher than 5 can be linked to a portion of metal ion elimination and the decrease in adsorption of metal ions at higher pH is mainly due to the formation of soluble hydroxyl complexes [57]. To prevent the formation of these complexes, all the experiments were carried at optimum solution pH 5.

4.2.2. Effect of initial metal ion concentration

Fig. 7 reveals the effect of the initial concentrations (10, 25, 50 and 100 mg L^{-1}) on the removal of Pb^{2+} aqueous

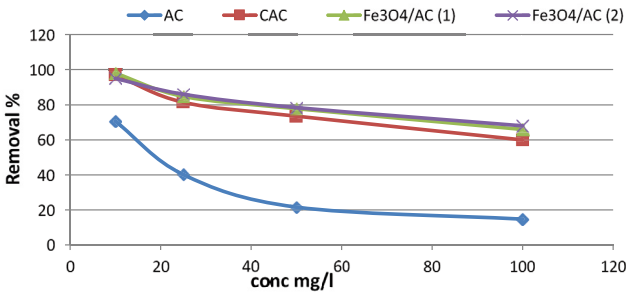

Fig. 7. Effect of initial metal ion concentration on the removal of Pb^{2+} by the different adsorbents at pH 5, 1 h, dose (2 g L^{-1}) of (AC, CAC and Fe_3O_4/AC(1)) and (1 g L^{-1}) of Fe_3O_4/AC(2), at room temperature (30°C ± 2°C) and shaking speed (200 rpm).

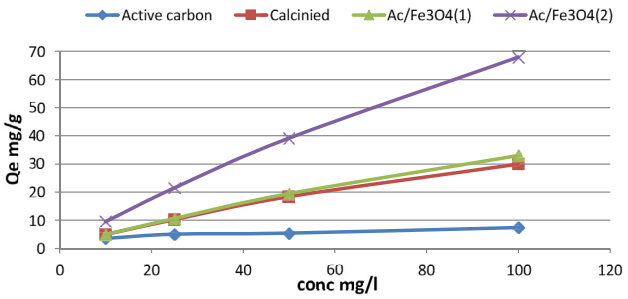

Fig. 8. Effect of initial metal ion concentration on the adsorption capacity of Pb^{2+} by the different adsorbents at pH 5, 1 h, dose (2 g L^{-1}) of (AC, CAC and Fe_3O_4/AC(1)) and (1 g L^{-1}) of Fe_3O_4/AC(2), at room temperature (30°C ± 2°C) and shaking speed (200 rpm).

solution using (2 g L^{-1}) from (AC, CAC and Fe_3O_4/AC(1)) and (1 g L^{-1}) from Fe_3O_4/AC(2) adsorbent materials at room temperature (30°C ± 2°C), 1 h contact time with a 200 rpm rotating shaking and pH = 5. It is indicated that the metal removal by both the sorbent materials employed decreased as the metal ion concentration in the solution was increased from 10 to 100 mg L^{-1} in the solution. Also the maximum Pb^{2+} removal percent obtained was achieved 70.6%, 97%, 98% and 95% at concentration 10 mg L^{-1} by using AC, CAC, Fe_3O_4/AC(1) and Fe_3O_4/AC(2), respectively. However, as the concentration of the metal ion increased, the adsorption capacity of the metal ion increased on all adsorbents. It increased from 3.53 to 7.35 mg g^{-1} for AC, 4.85 to 30 mg g^{-1} for CAC, 4.9 to 33 mg g^{-1} for Fe_3O_4/AC(1) and 9.5 to 68 mg g^{-1} for Fe_3O_4/AC(2). The increase in adsorption capacity (as shown in Fig. 8) can be explained on the basis that, an increase in initial metal ion concentration led to an increase in diffusion of Pb^{2+} ions from the solution phase to the surface of the adsorbents due to an increase in the driving force of metal ions causes collisions between metal ions and the surface of nanoparticles, resulting in an increase in adsorption capacity [58]. Similarly, Ibrahim et al. [59] used modified soda lignin (MSL) extracted from oil palm empty fruit bunches (EFB) for the removal of lead(II) ions from aqueous solutions. They found that the adsorption capacity of lead(II) ions increased from 2.47 to 21.54 mg g^{-1} as the initial concentration was increased from 5 to 100 ppm. The decrease in removal efficiency with an increase in metal ion concentration may be due to the restriction of adsorption sites present on the surface of adsorbent materials. This is attributed to the availability of more adsorption sites at low metal ion concentrations for the sorption of Pb^{2+} ions. At higher metal ion concentrations, the available active sites for the adsorption of metal ions become less and the percentage removal of metal ions depends on the initial metal ion concentration [4,50,60]. Therefore, to determine the effect of contact time and adsorbent dose, a metal ion concentration of 10 mg L^{-1} was used.

4.2.3. Effect of adsorbent dosage

The adsorbent dose is another important parameter, which influences the adsorption of metal ions onto the different adsorbents. The metal adsorption efficiency of the adsorbent materials with varying amounts for Pb^{2+} ions is shown in Fig. 9. The adsorbent dosage is 0.00625, 0.0125, 0.025, 0.0375, 0.05 and 0.1 g/25 mL of AC, CAC, Fe_3O_4/AC(1) and Fe_3O_4/AC(2) separately, for 10 mg L^{-1} of Pb^{2+} solution at 1 h contact time with a rotating shaker at 200 rpm, room temperature (30°C ± 2°C) and pH = 5.

Fig. 9 demonstrates that the percentage removal of metal ions increases with increase of adsorbent dose. This is due to the increase of surface area and the number of adsorption sites, which may be the reason for the removal of more ions at their surfaces [61]. At higher adsorbent doses, the adsorption capacity was lower (Fig. 10). At first all the adsorbent sites are available and later the adsorption rate was lowered that may be due to the lack of available active sites required for further uptake after reaching the equilibrium. The decrease in adsorption capacity as the adsorbent dose is increased may be due to particle interactions, such as aggregation, caused by high adsorbent concentrations, which reduce the active surface area of the adsorbent [39,62]. The removal percent of Pb^{2+} ions reached 79%, 100%, and 100% when using 4 g L^{-1} dose of AC, CAC and Fe_3O_4/AC(1), respectively, and 100% when using 1.5 g L^{-1} of Fe_3O_4/AC(2). The optimum dosages of AC, CAC and Fe_3O_4/AC(1) were used for the removal of lead is 2 and 1 g L^{-1} of Fe_3O_4/AC(2).

4.2.4. Effect of contact time

One of the most critical parameters that regulate adsorption processes is contact time. The effect of contact time on the removal of Pb^{2+} by the different adsorbent materials was then investigated in order to determine the optimum time taken to attain the equilibrium. Fig. 11 shows the adsorption of Pb^{2+} at pH 5 by using 2 g L^{-1} dose of AC, CAC, and Fe_3O_4/AC(1) and 1 g L^{-1} dose of Fe_3O_4/AC(2) at room temperature (30°C ± 2) and 10 mg L^{-1} metal ion concentration for the different time points; 2, 5, 10, 20, 40, 60, 90 and120 min. Fig. 11 depicts that the rate of Pb^{2+} ion removal increased over time, reaching saturation in about 2 h. Due to a rapid saturation of adsorption sites, lead showed a quick rate of adsorption within the first hour of adsorption, and the rate of removal percent became almost insignificant. The rapid adsorption may be due to the adsorption sites being more readily available at the start of the process. The adsorption sites were steadily occupied and began to saturate over time

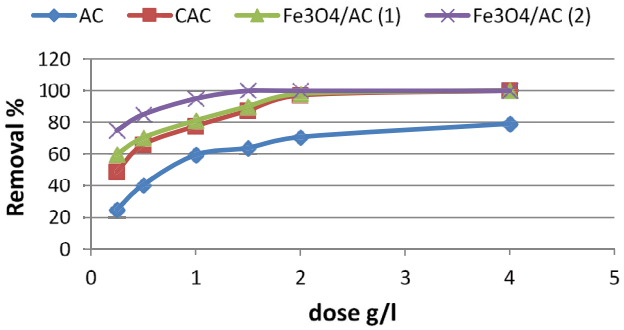

Fig. 9. Effect of adsorbent dose on the removal of Pb^{2+} by the different adsorbents at initial concentration of 10 mg L^{-1}, 1 h, pH 5, at room temperature (30°C ± 2°C) and shaking speed (200 rpm).

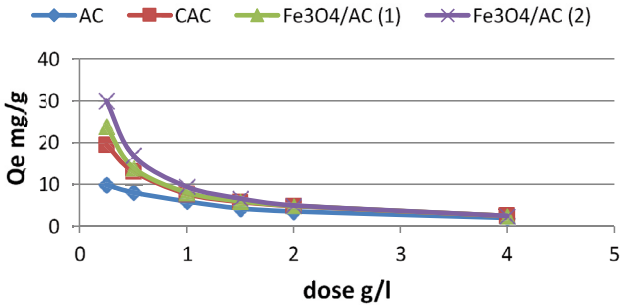

Fig. 10. Effect of adsorbent dose on the removal capacity of Pb^{2+} by the different adsorbents at initial concentration of 10 mg L^{-1}, 1 h, pH 5, at room temperature (30°C ± 2°C) and shaking speed (200 rpm).

due to a decline in the number of binding sites available suggesting monolayer coverage of the surface, resulting in a slower adsorption rate in the later stages [54,63,64].

After 5 min, about 51.45%, 65.17%, 72.9% and 75% of Pb^{2+} were removed from the solutions by using AC, CAC, Fe_3O_4/AC(1) and Fe_3O_4/AC(2), respectively. Within 120 min of operation about 78.75%, 99%, 99.9% and 99% of Pb^{2+} were removed from the solutions by using AC, CAC, Fe_3O_4/AC(1) and Fe_3O_4/AC(2), respectively. Taking into account that Fe_3O_4/AC(2) optimum dose used in all adsorption tests is 1 g L^{-1}. On the other hand, 2 g L^{-1} is the optimum dose used in AC, CAC and Fe_3O_4/AC(1) adsorbents.

4.2.5. Effect of temperature

The effect of temperature on the removal of Pb^{2+} by the different adsorbent materials was studied by varying the temperature in the range of 20°C–60°C again keeping all other process variables constant. Fig. 12 shows the removal of Pb^{2+} at pH 5 for 10 mg L^{-1} of Pb^{2+} solution at 1 h contact time with a rotating shaker at 200 rpm by using 2 g L^{-1} dose of AC, CAC and Fe_3O_4/AC(1) and 1 g L^{-1} dose of Fe_3O_4/AC(2) and 10 mg L^{-1} metal ion concentration for the different temperature points; 20°C, 30°C, 40°C, 50°C, and 60°C. The figure reveals that the adsorption of ions increased with an increase in temperature. The adsorption efficiency for

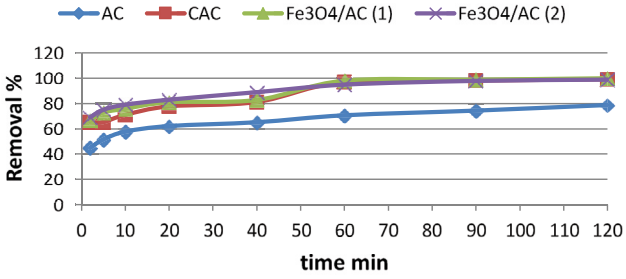

Fig. 11. Effect of contact time on the removal of Pb^{2+} by the different adsorbents at initial concentration of 10 mg L^{-1}, pH 5, dose (2 g L^{-1}) of (AC, CAC and Fe_3O_4/AC(1)) and (1 g L^{-1}) of Fe_3O_4/AC(2), at room temperature (30°C ± 2°C) and shaking speed (200 rpm).

Pb^{2+} increased from 59.12% to 74.2%, from 85.8% to 99%, from 96.3% to 100% and from 94% to 100% for AC, CAC, Fe_3O_4/AC(1) and Fe_3O_4/AC(2), respectively.

The results indicated that the adsorption process was endothermic in nature. This may be due to the fact that as the temperature rises, the mobility of the ions rises, increasing the interaction between the ions and the surface of the nanoparticles [22,37]. 30°C was chosen as the optimum temperature for all of the experiments because it is appropriate for practical application under field conditions. On the basis of the obtained data from section 4.2.1 to 4.2.5, a table (Table 3) has been prepared showing the optimum conditions needed for the highest removal efficiency of AC, CAC, Fe_3O_4/AC(1) and Fe_3O_4/AC(2) for removal of Pb^{2+} ions.

4.2.6. Pb^{2+} adsorption mechanism

By combining isothermal modelling of adsorption equilibrium data with surface characterization and pH studies, it is clear that the surface of Fe_3O_4/AC has a various functional groups which effectively chelate Pb^{2+} ions from water as indicated by FTIR analysis and the surface become rough and porous after activation of rice straw by the acid and addition of magnetite nanoparticles (Fe_3O_4-NPs) as shown by FE-SEM technique. pH studies also explained the adsorption process, Pb^{2+} adsorption was lower at lower pH but increased as pH increased. This behavior is due to the lower pH causes an abundance of hydronium ions (H_3O^+) in the solution, causing competition for adsorption onto adsorbent surface between hydronium ions and Pb^{2+} ions (Lead ions is present as Pb^{2+} and $Pb(OH)^+$ at lower pH), lowering the overall adsorption efficiency of these metal ions at lower pH. On the other hand, at higher pH levels the functional groups present on the surface of nanoparticles, such as carboxylic acid, hydroxyls, and phenol, are deprotonated, resulting in negative sites on the adsorbent surface. As a result of the electrostatic interaction between these negatively charged adsorption sites and positively charged Pb^{2+} ions, the adsorption is increased [56]. As a result, the formation of hydroxide precipitation ($Pb(OH)_2$) at pH higher than 5 can be linked to a portion of metal ion elimination [65]. Pb^{2+} adsorption was maximum at pH 5, hence that was chosen as the optimal pH [57,66]. The regression coefficient (R^2)

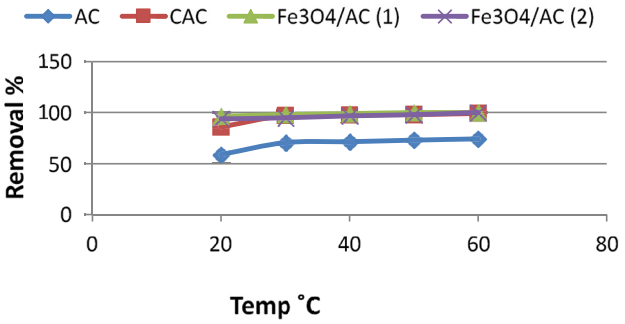

Fig. 12. Effect of temperature on the removal of Pb^{2+} by the different adsorbents at initial concentration of 10 mg L^{-1}, 1 h, dose (2 g L^{-1}) of (AC, CAC and Fe_3O_4/AC(1)) and (1 g L^{-1}) of Fe_3O_4/AC(2), pH 5 and shaking speed (200 rpm).

values of the Langmuir, Freundlich, and Temkin isothermal models also support this mechanism. The Freundlich isotherm model was shown to be more applicable than the other two, indicating that multi-layered physiosorption is the most common mechanism of Pb(II) ions adsorption heterogeneous adsorbent surfaces [67].

Fig. 13 represents the adsorption mechanism in graphical form.

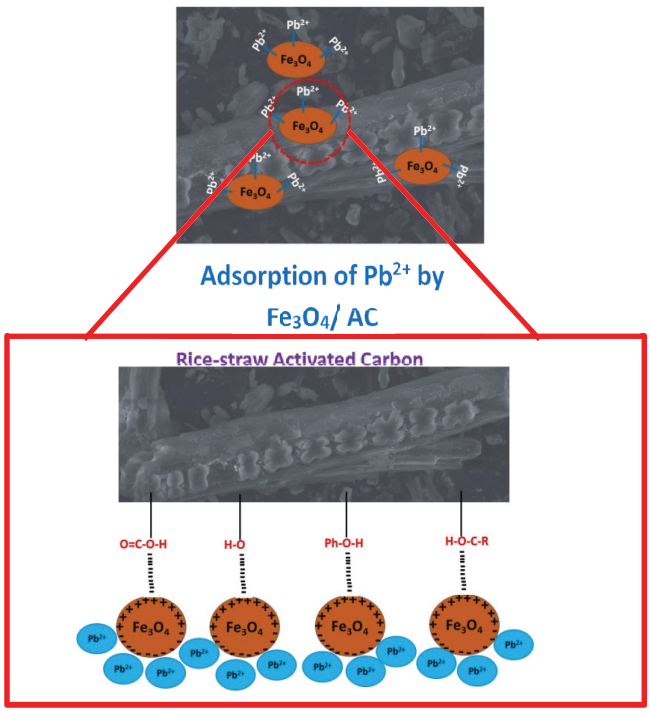

Fig. 13. Adsorption mechanism for the removal of Pb(II) by Fe_3O_4/AC(2).

4.2.7. Thermodynamic studies

Thermodynamic investigations can be used to determine if the adsorption mechanism is physical or chemical. The thermodynamic parameters for the removal of Pb^{2+} by the studied adsorbents were estimated using the following equations: standard Gibb's free energy ($\Delta G°$), standard enthalpy ($\Delta H°$), and standard entropy ($\Delta S°$).

$$\Delta G° = -RT\ln K \tag{3}$$

$$\Delta G° = \Delta H° - T\Delta S° \tag{4}$$

$$\ln K = -\frac{\Delta H°}{RT} + \frac{\Delta S°}{R} \tag{5}$$

$$K = \left(\frac{q_e}{C_e}\right) \tag{6}$$

where R (8.314 J mol^{-1} K^{-1}) is the universal gas constant, q_e is the amount of ion adsorbed on the surface of adsorbent (mg g^{-1}), C_e is equilibrium concentration (mg L^{-1}), T is temperature in Kelvins. Table 4 displays the thermodynamic parameters for adsorption of Pb^{2+} ions adsorbed on the surface of the studied adsorbents at different temperatures.

The negative value of ΔG in Table 4 indicates that the adsorption process is viable and spontaneous in nature. This is consistent with the Langmuir separation factor R_L results, which showed that the R_L values were between 0 and 1, that is, ($0 < R_L < 1$), and the Freundlich exponent n was likewise bigger than 1. The value of ΔG reduced as the temperature increased, showing that the increased temperature was beneficial to the adsorption process. The positive ΔH indicates that the adsorption process is endothermic and irreversible. The adsorption process is a mixture of two simple processes, Gibb's free energy ($\Delta G°$) and standard enthalpy ($\Delta H°$), with a positive value of ($\Delta S°$). Furthermore, positive $\Delta S°$ values suggested that the adsorbent surface was affine to Pb^{2+} ions and that the degrees of disorder and randomness at the solid-liquid interface were significant [33,68,69].

Table 3
Optimum conditions for the highest removal efficiency of AC, CAC, Fe_3O_4/AC(1) and Fe_3O_4/AC(2) for removal of Pb^{2+} ions

Adsorbent	pH	Dose (g L^{-1})	Initial concentration (mg L^{-1})	Contact time (min)	Temperature (°C)	Removal efficiency
AC	5	2	10	60	30	70.6%
CAC	5	2	10	60	30	97%
Fe_3O_4/AC(1)	5	2	10	60	30	98%
Fe_3O_4/AC(2)	5	1	10	60	30	95%

Table 4
Thermodynamic parameters for adsorption of Pb^{2+} ions by the different adsorbents at different temperatures

Adsorbent	T (K)	ΔG	ΔH	ΔS	R^2
	293	0.790	12.334	40.731	0.770
	303	–0.461			
AC	313	–0.590			
	323	–0.810			
	333	–1.006			
	293	–6.203	49.260	181.063	0.856
	303	–16.146			
CAC	313	–18.315			
	323	–19.783			
	333	–24.880			
	293	–14.396	119.628	423.55	0.901
	303	–18.558			
Fe_3O_4/AC(1)	313	–23.386			
	323	–38.430			
	333	–54.308			
	293	–15.437	37.038	147.764	0.941
	303	–17.083			
Fe_3O_4/AC(2)	313	–20.434			
	323	–23.762			
	333	–29.364			

4.2.8. Adsorption isotherms

The aim of adsorption isotherms is to find a relationship between the adsorbate concentration in the bulk and the amount adsorbed at the interface [62]. Batch adsorption data was described using Langmuir, Freundlich and Temkin models [70]. Monolayer adsorption is defined by the Langmuir isotherm, which assumes homogeneous sorption sites and sorption energies on the surface of adsorbents [35]. It is also believed that once a metal ion has occupied a site, no further sorption will take place [71]. Both the Langmuir and Freundlich isotherm models have been shown to be adequate for explaining short-term and mono component metal ion adsorption by various sorbent materials. The linear form of Langmuir model and its dimensionless constant separation factor R_L is expressed in Eqs. (7) and (8) [72].

$$\frac{C_e}{Q_e} = \frac{1}{Q_o b} + \frac{C_e}{Q_o} \tag{7}$$

$$R_L = \frac{1}{1 + bC_i} \tag{8}$$

where Q_o (mg g^{-1}) is the maximum Langmuir adsorption capacity and b (L mg^{-1}) is the Langmuir constant related to free energy. A plot of C_e vs. C_e/Q_e for using AC, CAC, Fe_3O_4/AC(1) and Fe_3O_4/AC(2) for Pb^{2+} is shown in Fig. 14. The Langmuir constants Q_o and b were calculated from the

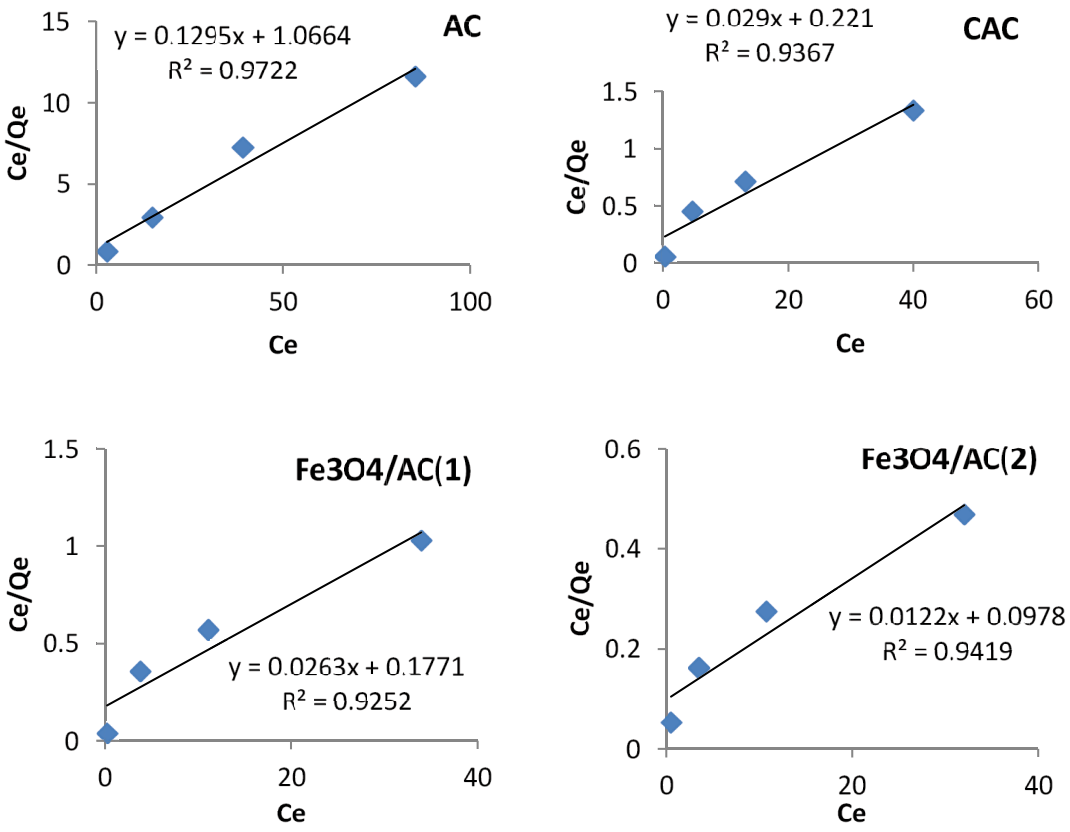

Fig. 14. Langmuir isotherm model plots for removal of Pb^{2+} ions using different adsorbents.

slope and intercept of the Langmuir plot of C_e vs. C_e/Q_e is represented in Table 5.

The Langmuir treatment is based on the idea that total adsorption corresponds to a saturated mono-layer of adsorbate molecules on the adsorbent surface, with constant adsorption energy and no adsorbate migrate into the plane of the surface. The Langmuir constant b quantifies the affinity between the adsorbent and the adsorbate, and the lower the value obtained, the greater the metal's affinity for the adsorbent material. Furthermore, the adsorption capacity can imply a relationship between the adsorbent's surface area and porosity, that is, the higher the surface area and pore volume, the greater the metal ion adsorption capacity [73]. The value of R_L has four possibilities: $0 < R_L < 1$ for favorable adsorption, $R_L > 1$ for unfavorable adsorption, $R_L = 1$ for linear adsorption, and $R_L = 0$ for irreversible adsorption. In this study, the values for R_L obtained for the studied system indicate the favorability of Pb^{2+} ions adsorption onto all adsorbents. Moreover, the obtained R^2 value for Pb^{2+} using AC; (0.972), CAC; (0.937), Fe_3O_4/AC(1); (0.925), and Fe_3O_4/AC(2); (0.942), respectively. For AC, the R^2 value of Langmuir was higher than other adsorbents and Freundlich model thus indicating that Pb^{2+} adsorption by AC is better fitted with the Langmuir model, thereby indicating monolayer adsorption. The maximum adsorption capacity calculated by Langmuir model of Fe_3O_4/AC(2) for adsorption of Pb^{2+} was compared with other adsorbents in the literature and the values are given in Table 6. It is clear that the adsorption capacity of Fe_3O_4/AC(2) nanocomposite is comparable with other adsorbents suggesting that, it is effective in removing Pb^{2+} from aqueous solutions [65,74–76].

Freundlich adsorption model assumes that adsorbents have a heterogeneous surface containing sites with various adsorption capacities [77]. It also implies that stronger binding sites are occupied first, and that as the degree of occupation increases, the binding strength decreases [22]. The linearized Freundlich isotherm is given by Eq. (9)

$$\log Q_e = \log k_f + \frac{1}{n}\log C_e \tag{9}$$

where k_f (mg g^{-1}) is the Freundlich constant indicating adsorption capacity, n (L mg^{-1}) is the adsorption strength that is the measure of the change in adsorbate affinity with a change in adsorption density. The Freundlich constants (k_f and n) were calculated from the slope and intercept of the plot of C_e vs. $\log q_e$ (Table 5). In addition, the magnitude of n indicates the adsorption favorability. In other words, if the n value obtained is between 2 and 10, it suggests a significant adsorption characteristic, whereas values between 1 and 2 indicate a moderately difficult adsorption characteristic, and values less than 1 indicate a poor adsorption characteristic [78]. A plot of $\log Q_e$ vs. $\log C_e$ for using AC, CAC, Fe_3O_4/AC(1) and Fe_3O_4/AC(2) for Pb^{2+} ions is shown in Fig. 15. The values obtained for the slopes and intercepts of these plots are presented in Table 5. The adsorption intensity (n) values were between 2 and 10 for all adsorbent materials, which indicates a favorable process and the surface of sorbent materials was heterogeneous. The values of (R^2) in Freundlich model for Pb^{2+} using AC; (0.915), CAC; (0.972), Fe_3O_4/AC(1); (0.966), and Fe_3O_4/AC(2); (0.997), respectively were higher as compared to Langmuir model thus, indicating that Freundlich model fitted the data well confirming multilayer adsorption. Except in the case of Pb^{2+} by AC in Langmuir R^2 value (0.972) is higher than that of Freundlich (0.915).

The Temkin isotherm model predicts that adsorption energy decreases linearly with surface coverage because of adsorbent–adsorbate interactions. The Temkin isotherm model's linear form is as follows [40]:

$$q_e = \frac{RT}{b}\ln K_t + \frac{RT}{b}\ln C_e \tag{10}$$

where T is the absolute temperature (Kelvin) and R is the universal gas constant (J mol^{-1} K^{-1}). b is the Temkin constant related to the heat of adsorption and K_T is the equilibrium

Table 6
Comparison of monolayer adsorption capacity of different adsorbents reported in literature used for Pb(II) remove

Adsorbent	q_e (mg g^{-1})	References
Bentonite	7.56	[74]
Activated carbon	6.68	[74]
Blast furnace slag	5.52	[74]
Fly ash	04.98	[74]
Kaolin	04.50	[74]
Bagasse fly ash	2.5	[65]
Sawdust	3	[75]
Tea waste	2	[75]
Peach stone	0.0023	[75]
Apricot stone	0.0013	[75]
Magnetic oak wood char	10.13	[76]
Rice husk biochar	1.84	[76]
Fe_3O_4/AC(2)	10.225	This study

Table 5
Freundlich, Langmuir and Temkin isotherms' constants for Pb^{2+} adsorption onto the studied adsorbents

Metal	Adsorbent	Langmuir isotherm model				Freundlich isotherm model				Temkin isotherm model		
		q_{max}	K_a	R_L	R^2	k_f	$1/n$	n	R^2	b	K_T (L mg^{-1})	R^2
Pb^{2+}	AC	0.938	8.234	0.012	0.972	2.820	0.202	4.946	0.915	2446	1.461	0.905
	CAC	4.525	7.621	0.013	0.937	6.979	0.396	2.708	0.972	525	1.654	0.843
	Fe_3O_4/AC(1)	5.627	6.757	0.015	0.925	8.058	0.365	2.737	0.966	501	1.527	0.820
	Fe_3O_4/AC(2)	10.225	0.957	0.095	0.942	12.715	0.474	2.109	0.997	186	2.393	0.893

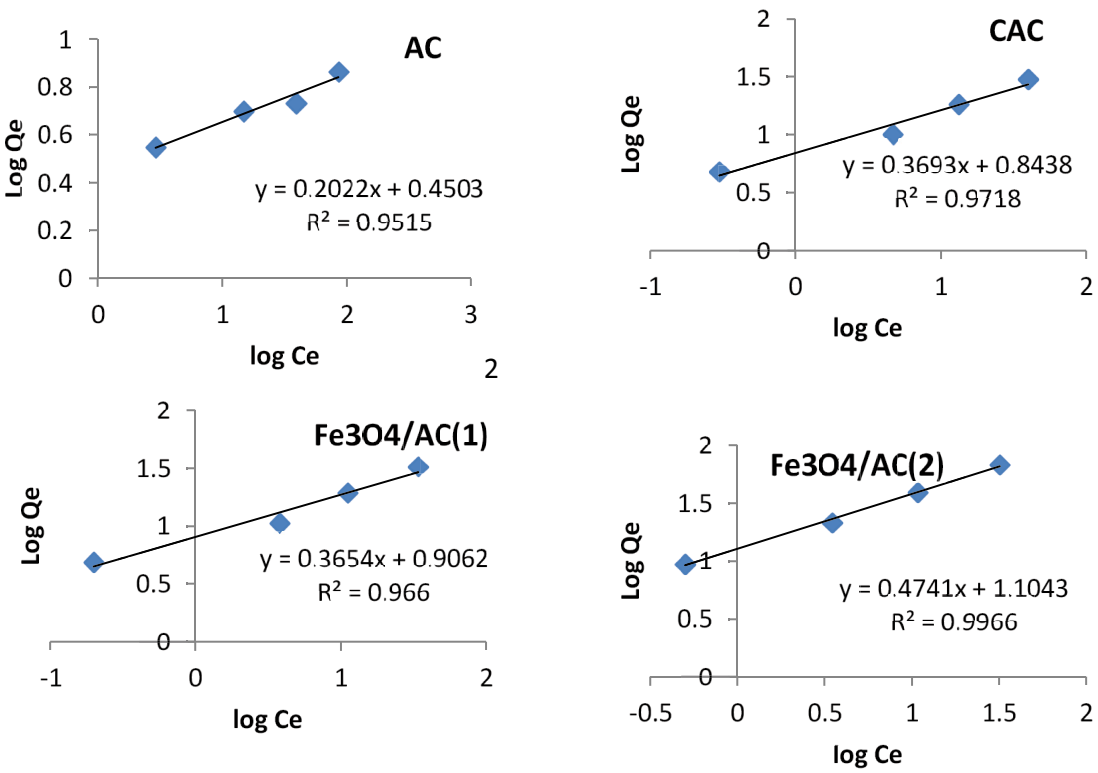

Fig. 15. Freundlich isotherm model plots for removal of Pb^{2+} ions using different adsorbents.

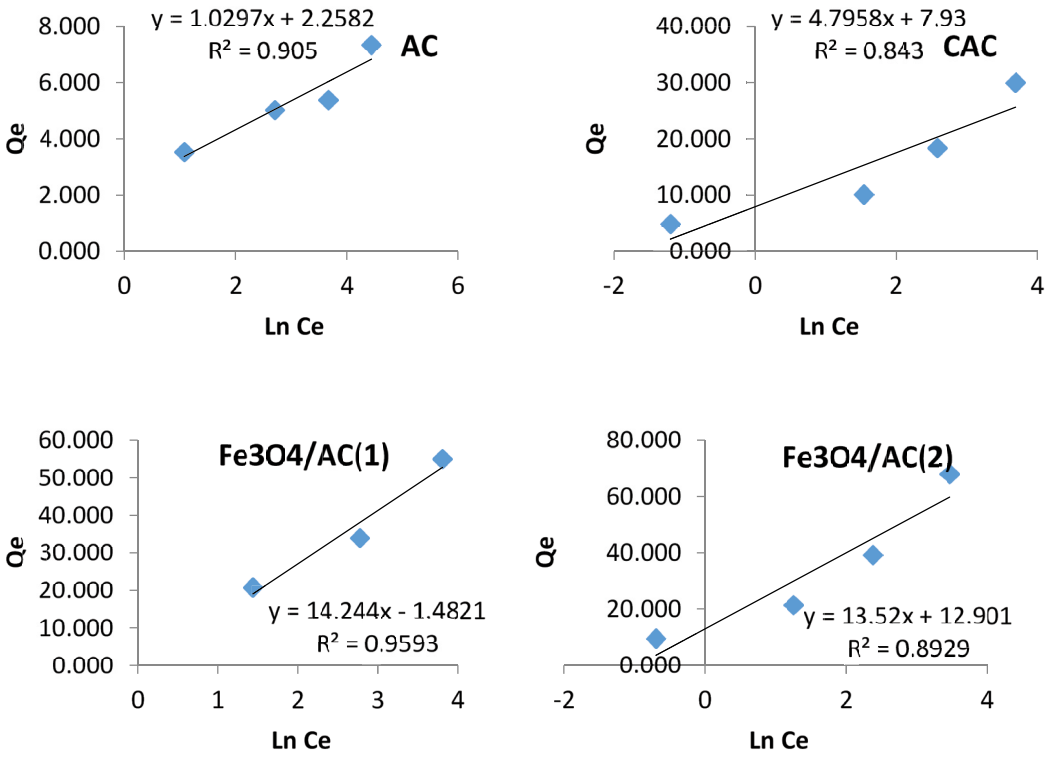

Fig. 16. Temkin isotherm model plots for removal of Pb^{2+} using different adsorbents.

binding constant (L mg^{-1}) corresponding to the maximum binding energy. The values of these parameters are calculated and presented in Table 5. A plot of q_e vs. lnC_e enables the determination of the isotherm constant K_T and RT/b as shown in Fig. 16.

4.2.9. Adsorption kinetics

Adsorption kinetics, which is dependent on the physical and chemical properties of the adsorbent, describes the rate of reaction and reaction pathways. Three separate kinetic models, the pseudo-first-order, pseudo-second-order equations and intraparticle diffusion, were used to test the experimental results. Pseudo-first-order kinetic model was used to explain adsorption in a solid–liquid system Eq. (11) [77]. One metal ion is sorbed onto one sorption site on the adsorbent's surface, according to this model:

$$\log\left(q_e - q_t\right) = \log q_e - \frac{k_1}{2.303}t \tag{11}$$

where q_e is the adsorption capacity at equilibrium time and q_t (mg g^{-1}) is the adsorption capacity at time t (min), and k_1 (min^{-1}) is the equilibrium rate constant for pseudo-first-order model. The value of k_1 is derived from the slope of the linear plots of log (q_e – q_t) vs. time (min) as shown in Fig. 17. The values of q_e (experimental) (mg g^{-1}), q_e (calculated) (mg g^{-1}), k_1 (min^{-1}) and R^2 for Pb^{2+} by AC, calcined AC, Fe_3O_4/AC(1) and Fe_3O_4/AC(2) are given in Table 7. The table shows that the regression coefficient (R^2) values for the pseudo-first-order model are poor, and the calculated q_e values are not close to experimental q_e values, suggesting that this model does not match our data well. Therefore, the adsorption of Pb^{2+} ions by AC, CAC, Fe_3O_4/AC(1) and Fe_3O_4/AC(2) was examined using a pseudo-second-order model.

The pseudo-second-order model (Eq. 12) assumes that, on the surface of the adsorbent, one metal ion is sorbed into two sorption sites. The chemisorption kinetics of liquid solutions has been studied using this model. k_2 (g mg^{-1} min^{-1}) is the equilibrium rate constant and k_2q_e is the initial adsorption rate (mg g^{-1} min^{-1}) for pseudo-second-order model [79]. The values of $1/k_2q_e^2$ and $1/q_e$ are derived from the intercept and slope of the linear plots of t/q_t vs. time (min) as shown in Fig. 18, which leads to calculation of the values of k_2 and q_e (calculated) [59]:

$$\frac{t}{q_t} = \frac{1}{k_2q_e^2} + \frac{1}{q_e}t \tag{12}$$

The values of q_e (experimental) (mg g^{-1}), q_e (calculated) (mg g^{-1}); k_2 (g mg^{-1} min^{-1}) and R^2 of Pb^{2+} removal by AC, CAC, Fe_3O_4/AC(1) and Fe_3O_4/AC(2) are given in Table 7. Investigations of the use of AC, CAC, Fe_3O_4/AC(1) and Fe_3O_4/AC(2) as sorbent for removal of Pb^{2+} ions from

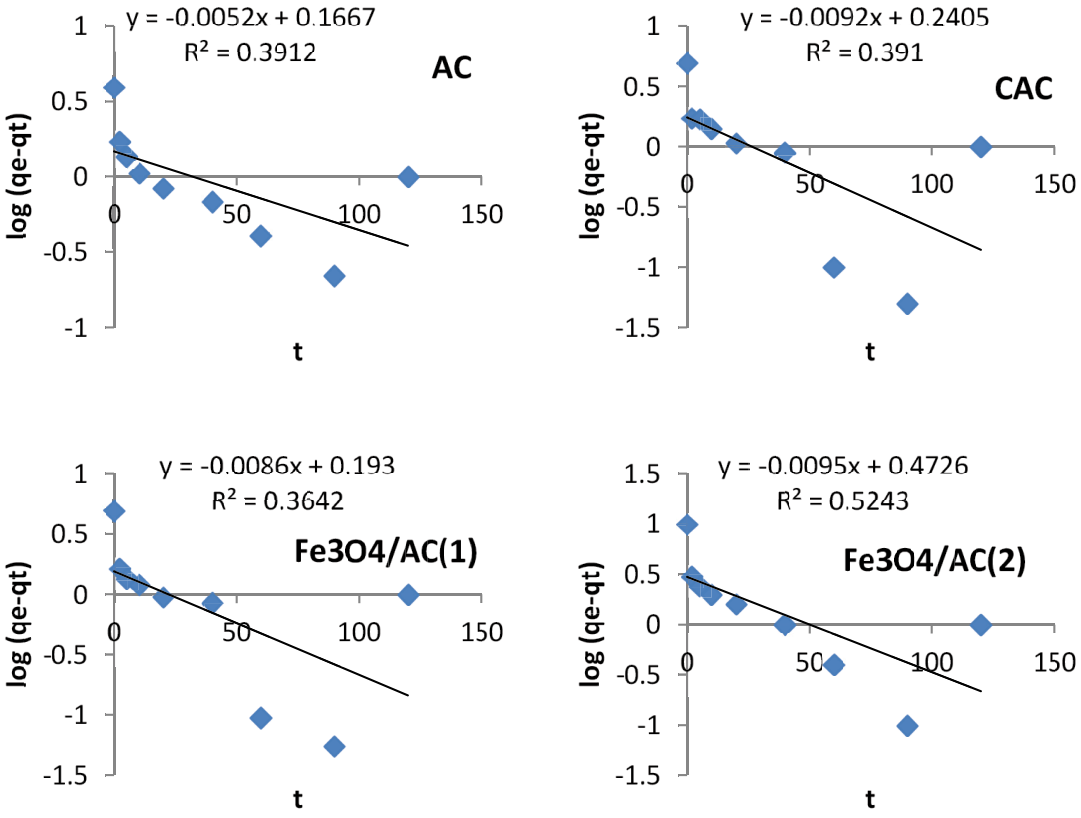

Fig. 17. The pseudo-first-order rate for adsorption of Pb^{2+} by different adsorbents.

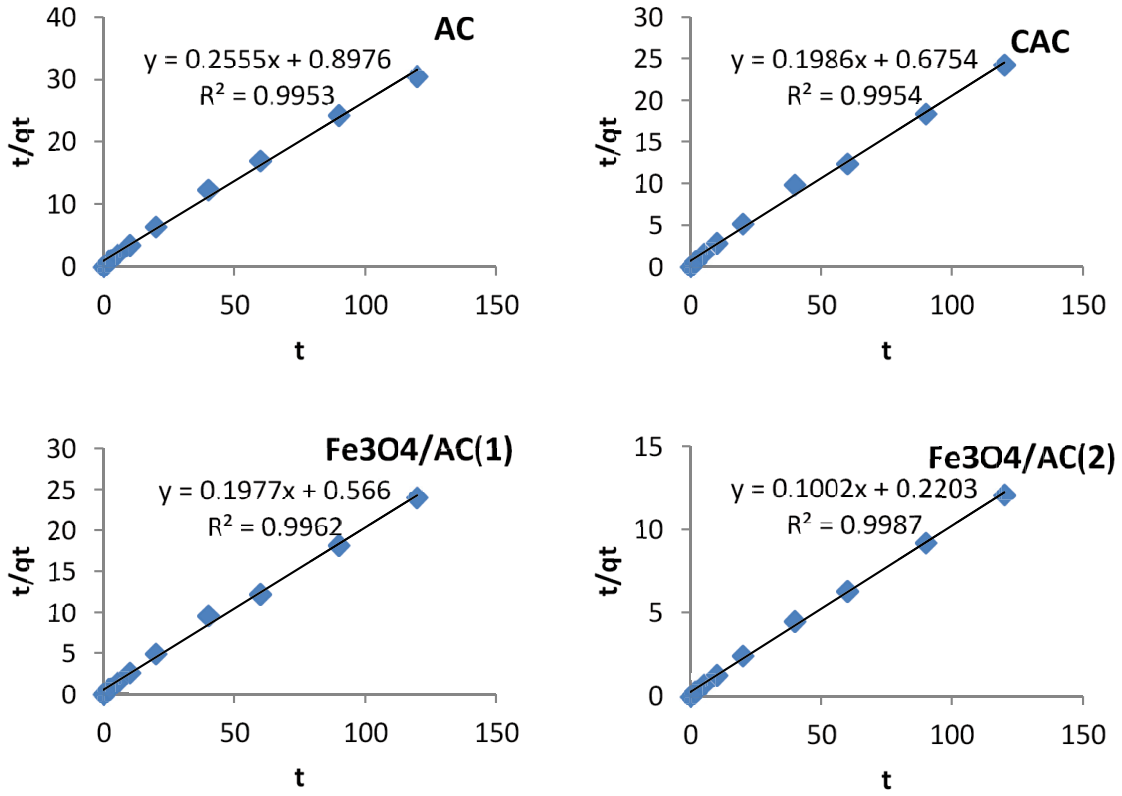

Fig. 18. The pseudo-second-order rate for adsorption of Pb^{2+} by different adsorbents.

Table 7
Pseudo-first-order, pseudo-second-order and intraparticle diffusion kinetic models for the removal of Pb^{2+} by the studied adsorbents

		Pseudo-first-order kinetic model				Pseudo-second-order kinetic model				Intraparticle diffusion model		
Metal	Adsorbent	q_{exp}	$q_{e,cal}$	k_1	R^2	q_{exp}	$q_{e,cal}$	k_2	R^2	K_{1d} (mg g^{-1} $min^{-1/2}$)	C (mg g^{-1})	R^2
Pb	AC	3.938	1.468	0.012	0.391	3.938	3.914	0.073	0.995	0.162	2.228	0.957
	CAC	4.95	1.740	0.021	0.319	4.95	5.035	0.058	0.995	0.204	2.92	0.944
	Fe_3O_4/AC(1)	4.995	1.560	0.020	0.364	4.995	5.085	0.691	0.996	0.179	3.205	0.938
	Fe_3O_4/AC(2)	9.9	2.969	0.022	0.524	9.9	9.980	0.046	0.999	0.314	6.789	0.961

Table 8
Comparison of adsorption capacity of Fe_3O_4/AC(1) and Fe_3O_4/AC(2) with other adsorbents

Adsorbents	Adsorption capacity (mg g^{-1})	References
Fe_3O_4 magnetite activated carbon composite	2.19	[81]
Iron oxide nanoparticles	18.59	[82]
Iron oxide nanoparticles	17.6	[83]
Fe_3O_4/SC	15	[84]
RHC-mag-CN	16	[85]
Iron oxide NPs embedded in orange peel pith	5.37	[86]
Fe_3O_4/AC	4.4	[22]
Fe_3O_4/AC(1)	33	This study
Fe_3O_4/AC(2)	68	This study

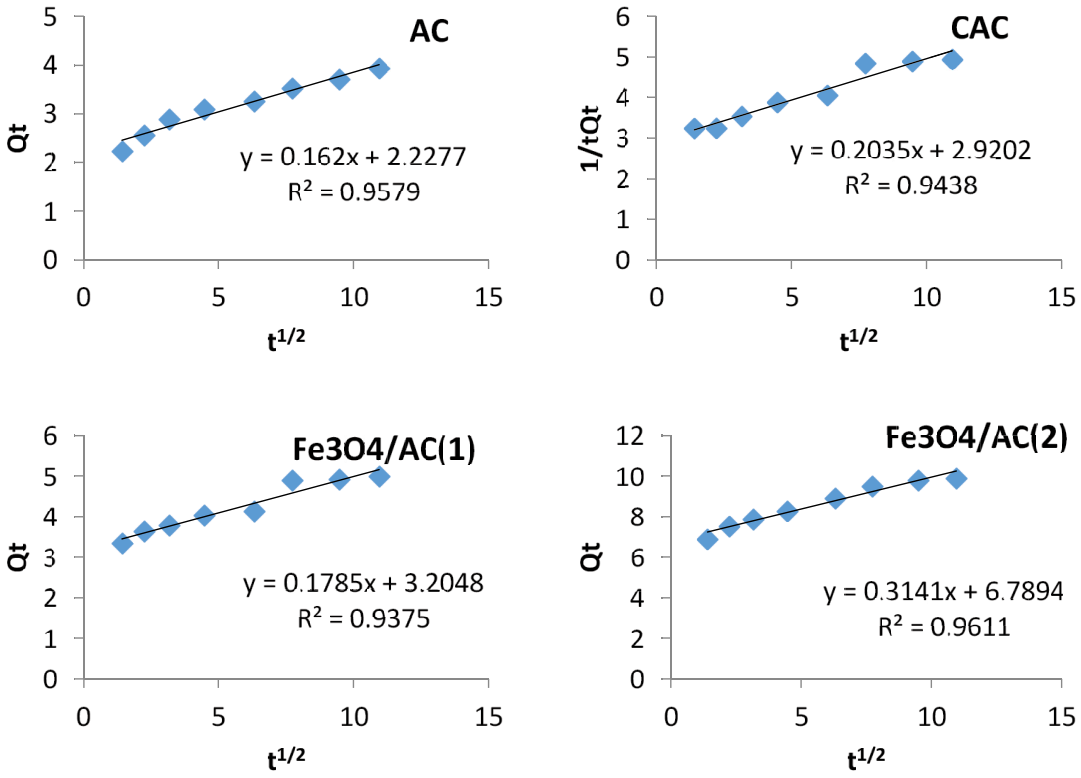

Fig. 19. The intraparticle diffusion for adsorption of Pb^{2+} onto the studied adsorbents.

solution indicated that the process was a second-order process due to high regression value of R^2 are (0.995, 0.995, 0.996 and 0.999), in case of using AC, CAC, Fe_3O_4/AC(1) and Fe_3O_4/AC(2), respectively. In addition, values of q_e (experimental) and q_e (calculated) are close to each other, indicating that the pseudo-second-order model better fits the data than the pseudo-first-order model.

The Weber–Morris model (1963) is used to investigate the adsorption kinetics and determine the role of diffusion in the adsorption process. The transport of ions from bulk solution to solid phase is described by this model (Eq. 13) [80]. It is assumed that the adsorption process takes place in two stages. The first straight segment illustrates macro-pore diffusion (i.e., diffusion of heavy metals from the solution to the nano-sorbent's exterior surface, also known as external diffusion), whereas the second depicts micro-pore diffusion (diffusion of heavy metals from the nano-sorbent's surface into the pores):

$$q_t = K_{id} t^{1/2} + C \tag{13}$$

where q_t is the metal ion adsorbed (mg g^{-1}) at time t (min), K_{id} (mg g^{-1} $min^{-1/2}$) is the rate constant for intraparticle diffusion which can be obtained from the slope of the straight line (slope of the plots between q_t and $t^{1/2}$) and C is the thickness of the boundary layer obtained from the intercept of the plots between q_t and time (min). The values of K_{id} and C are given in Table 7. Greater the value of C, greater is the effect of the boundary layer. If intraparticle diffusion occurs, the relationship between q_t and $t^{1/2}$ will be linear as shown in Fig. 19, with the line passing through the origin. However, because the line did not pass through the origin in our case, it is likely that another process is involved in the adsorption. The calculated intraparticle diffusion rate constants are not zero, implying that the adsorption process may not be controlled by the intraparticle diffusion model [33,41].

4.2.10. Comparison of adsorption capacity with other adsorbents

The maximum adsorption capacity of Fe_3O_4/AC adsorbent for the removal of Pb^{2+} was compared with other adsorbents reported in the literature and the values are given in Table 8. It is clear that the adsorption capacity of Fe_3O_4/AC is comparable with other nanomaterials suggesting that, it is effective in removing Pb^{2+} from aqueous solutions [22,81–86].

5. Conclusion

In this study, the adsorption potential of AC, CAC, Fe_3O_4/AC(1) and Fe_3O_4/AC(2) adsorbent materials was investigated for the removal of Pb^{2+} ions. The XRD analysis of Fe_3O_4/AC(1,2) confirmed the presence of magnetite phase which is crystalline in nature and has the cubic structure, on the other hand, activated carbon didn't show any specific peak confirming that the AC is amorphous in nature in AC and CAC samples. The optimum adsorption pH was

found to be 5 for Pb^{2+}. The removal efficiency of the adsorbents decreased with an increase in the concentration, that is, 70.6%–14.69%, 97%–60%, 98%–66% and 95%–68% for Pb^{2+} by AC, CAC, Fe_3O_4/AC(1) and Fe_3O_4/AC(2), respectively. The adsorption efficiency for Pb^{2+} by Fe_3O_4/AC(2) was high in the beginning of the experiments as indicated by 75% removal in the first 5 min. The optimum conditions for the highest removal efficiency of AC, CAC, Fe_3O_4/AC(1) and Fe_3O_4/AC(2) for removal of heavy metal Pb^{2+} was pH = 5, room temperature (30°C ± 2°C), initial metal ion concentration = 10 mg L^{-1} contact time = 60 min and dose of 2 g L^{-1} by AC, CAC and Fe_3O_4/AC(1) and 1 g L^{-1} by Fe_3O_4/AC(2). The maximum Freundlich adsorption capacity for Pb^{2+} ions was 2.820, 6.979, 8.058 and 12.715 mg g^{-1} by AC, CAC, Fe_3O_4/AC(1) and Fe_3O_4/AC(2), respectively.

Acknowledgements

M. El-Sheeta is very grateful for the Academy of Scientific Research and Technology (ASRT), Egypt for the SNG scholarship to achieve this work towards her M.Sc. degree.

References

[1] B. Hayati, A. Maleki, F. Najafi, H. Daraei, F. Gharibi, G. McKay, Synthesis and characterization of PAMAM/CNT nanocomposite as a super-capacity adsorbent for heavy metal (Ni^{2+}, Zn^{2+}, As^{3+}, Co^{2+}) removal from wastewater, J. Mol. Liq., 224 (2016) 1032–1040.

[2] M.-E. Lee, J.H. Park, J.W. Chung, C.-Y. Lee, S. Kang, Removal of Pb and Cu ions from aqueous solution by Mn_3O_4-coated activated carbon, J. Ind. Eng. Chem., 21 (2015) 470–475.

[3] F. Ghorbani, S. Kamari, S. Zamani, S. Akbari, M. Salehi, Optimization and modeling of aqueous Cr(VI) adsorption onto activated carbon prepared from sugar beet bagasse agricultural waste by application of response surface methodology, Surf. Interfaces, 18 (2020) 100444, doi: 10.1016/j.surfin.2020.100444.

[4] M. Ghasemi, M. Naushad, N. Ghasemi, Y. Khosravi-fard, Adsorption of Pb(II) from aqueous solution using new adsorbents prepared from agricultural waste: adsorption isotherm and kinetic studies, J. Ind. Eng. Chem., 20 (2014) 2193–2199.

[5] L. Mouni, D. Merabet, A. Bouzaza, L. Belkhiri, Adsorption of Pb(II) from aqueous solutions using activated carbon developed from Apricot stone, Desalination, 276 (2011) 148–153.

[6] M. Arbabi, S. Hemati, M. Amiri, Removal of lead ions from industrial wastewater: a review of removal methods, Int. J. Epidemiol. Res., 2 (2015) 105–109.

[7] W. Yang, Q. Tang, J. Wei, Y. Ran, L. Chai, H. Wang, Enhanced removal of Cd(II) and Pb(II) by composites of mesoporous carbon stabilized alumina, Appl. Surf. Sci., 369 (2016) 215–223.

[8] T.S. Anirudhan, S.S. Sreekumari, Adsorptive removal of heavy metal ions from industrial effluents using activated carbon derived from waste coconut buttons, J. Environ. Sci., 23 (2011) 1989–1998.

[9] L. Joseph, B.-M. Jun, J.R.V. Flora, C.M. Park, Y. Yoon, Removal of heavy metals from water sources in the developing world using low-cost materials: a review, Chemosphere, 229 (2019) 142–159.

[10] R. Hoseinzadeh Hesas, W.M.A. Wan Daud, J.N. Sahu, A. Arami-Niya, The effects of a microwave heating method on the production of activated carbon from agricultural waste: a review, J. Anal. Appl. Pyrolysis, 100 (2013) 1–11.

[11] S. Mashhadi, R. Sohrabi, H. Javadian, M. Ghasemi, I. Tyagi, S. Agarwal, V.K. Gupta, Rapid removal of Hg(II) from aqueous solution by rice straw activated carbon prepared by microwave-assisted H_2SO_4 activation: kinetic, isotherm and thermodynamic studies, J. Mol. Liq., 215 (2016) 144–153.

[12] H. Zhang, Y.-J. Wang, F. Lü, L.-N. Chai, L.-M. Shao, P.-J. He, Effects of dilute acid pretreatment on physicochemical characteristics and consolidated bioprocessing of rice straw, Waste Biomass Valorization, 6 (2015) 217–223.

[13] R. Sharma, B. Singh, Removal of Ni(II) ions from aqueous solutions using modified rice straw in a fixed bed column, Bioresour. Technol., 146 (2013) 519–524.

[14] P. Kaur, M.S. Taggar, A. Kalia, Characterization of magnetic nanoparticle–immobilized cellulases for enzymatic saccharification of rice straw, Biomass Convers. Biorefin., 11 (2021) 955–969.

[15] D. Dias, N. Lapa, M. Bernardo, W. Ribeiro, I. Matos, I. Fonseca, F. Pinto, Cr(III) removal from synthetic and industrial wastewaters by using co-gasification chars of rice waste streams, Bioresour. Technol., 266 (2018) 139–150.

[16] Y. Dai, Q. Sun, W. Wang, L. Lu, M. Liu, J. Li, S. Yang, Y. Sun, K. Zhang, J. Xu, W. Zheng, Z. Hu, Y. Yang, Y. Gao, Y. Chen, X. Zhang, F. Gao, Y. Zhang, Utilizations of agricultural waste as adsorbent for the removal of contaminants: a review, Chemosphere, 211 (2018) 235–253.

[17] S. Mashhadi, H. Javadian, M. Ghasemi, T.A. Saleh, V.K. Gupta, Microwave-induced H_2SO_4 activation of activated carbon derived from rice agricultural wastes for sorption of methylene blue from aqueous solution, Desal. Water Treat., 57 (2016) 21091–21104.

[18] M.A. Yahya, Z. Al-Qodah, C.W. Zanariah Ngah, Agricultural bio-waste materials as potential sustainable precursors used for activated carbon production: a review, Renewable Sustainable Energy Rev., 46 (2015) 218–235.

[19] O. Ioannidou, A. Zabaniotou, Agricultural residues as precursors for activated carbon production—a review, Renewable Sustainable Energy Rev., 11 (2007) 1966–2005.

[20] G. Özsin, M. Kılıç, E. Apaydın-Varol, A.E. Pütün, Chemically activated carbon production from agricultural waste of chickpea and its application for heavy metal adsorption: equilibrium, kinetic, and thermodynamic studies, Appl. Water Sci., 9 (2019), doi: 10.1007/s13201-019-0942-8.

[21] S. Chakraborty, S. Chowdhury, P. Das Saha, Artificial neural network (ANN) modeling of dynamic adsorption of crystal violet from aqueous solution using citric-acid-modified rice (*Oryza sativa*) straw as adsorbent, Clean Technol. Environ. Policy, 15 (2013) 255–264.

[22] M. Jain, M. Yadav, T. Kohout, M. Lahtinen, V.K. Garg, M. Sillanpää, Development of iron oxide/activated carbon nanoparticle composite for the removal of Cr(VI), Cu(II) and Cd(II) ions from aqueous solution, Water Resour. Ind., 20 (2018) 54–74, doi: 10.1016/j.wri.2018.10.001.

[23] Ö. Gerçel, A. Özcan, A. Safa Özcan, H. Ferdi Gerçel, Preparation of activated carbon from a renewable bio-plant of *Euphorbia rigida* by H_2SO_4 activation and its adsorption behavior in aqueous solutions, Appl. Surf. Sci., 253 (2007) 4843–4852.

[24] B. Singha, S.K. Das, Adsorptive removal of Cu(II) from aqueous solution and industrial effluent using natural/agricultural wastes, Colloids Surf., B, 107 (2013) 97–106.

[25] T. Khan, M. Hasnain Isa, M.R. Ul Mustafa, H. Yeek-Chia, L. Baloo, T.S.B. Abd Manana, M.O. Saeed, Cr(VI) adsorption from aqueous solution by an agricultural waste based carbon, RSC Adv., 6 (2016) 56365–56374.

[26] N.-H. Hsu, S.-L. Wang, Y.-H. Liao, S.-T. Huang, Y.-M. Tzou, Y.-M. Huang, Removal of hexavalent chromium from acidic aqueous solutions using rice straw-derived carbon, J. Hazard. Mater., 171 (2009) 1066–1070.

[27] C.G. Rocha, D.A.M. Zaia, R.V. da S. Alfaya, A.A. da S. Alfaya, Use of rice straw as biosorbent for removal of Cu(II), Zn(II), Cd(II) and Hg(II) ions in industrial effluents, J. Hazard. Mater., 166 (2009) 383–388.

[28] E.I. El-Shafey, Removal of Zn(II) and Hg(II) from aqueous solution on a carbonaceous sorbent chemically prepared from rice husk, J. Hazard. Mater., 175 (2010) 319–327.

[29] T.C. Prathna, S.K. Sharma, M. Kennedy, Nanoparticles in household level water treatment: an overview, Sep. Purif. Technol., 199 (2018) 260–270.

[30] Y. Panahi, H. Mellatyar, M. Farshbaf, Z. Sabet, T. Fattahi, A. Akbarzadehe, Biotechnological applications of nanomaterials

for air pollution and water/wastewater treatment, Mater. Today:. Proc., 5 (2018) 15550–15558.
[31] G.A.P. Mateus, M.P. Paludo, T.R.T. dos Santos, M.F. Silva, L. Nishi, M.R. Fagundes-Klen, R.G. Gomes, R. Bergamasco, Obtaining drinking water using a magnetic coagulant composed of magnetite nanoparticles functionalized with *Moringa oleifera* seed extract, J. Environ. Chem. Eng., 6 (2018) 4084–4092.
[32] S. Parlayıcı, E. Pehlivan, Removal of metals by Fe_3O_4 loaded activated carbon prepared from plum stone (*Prunus nigra*): kinetics and modelling study, Powder Technol., 317 (2017) 23–30.
[33] M. Ghasemi, Mu. Naushad, N. Ghasemi, Y. Khosravi-fard, A novel agricultural waste based adsorbent for the removal of Pb(II) from aqueous solution: kinetics, equilibrium and thermodynamic studies, J. Ind. Eng. Chem., 20 (2014) 454–461.
[34] P. Shekinah, K. Kadirvelu, P. Kanmani, P. Senthilkumar, V. Subburam, Adsorption of lead(II) from aqueous solution by activated carbon prepared from *Eichhornia*, J. Chem. Technol. Biotechnol., 77 (2002) 458–464.
[35] H. Amer, A. El-Gendy, S. El-Haggar, Removal of lead(II) from aqueous solutions using rice straw, Water Sci. Technol., 76 (2017) 1011–1021.
[36] M.J.E. Zarandi, M.R. Sohrabi, M. Khosravi, N. Mansouriieh, M. Davallo, A. Khosravan, Optimizing Cu(II) removal from aqueous solution by magnetic nanoparticles immobilized on activated carbon using Taguchi method, Water Sci. Technol., 74 (2016) 38–47.
[37] M.H. Fatehi, J. Shayegan, M. Zabihi, I. Goodarznia, Functionalized magnetic nanoparticles supported on activated carbon for adsorption of Pb(II) and Cr(VI) ions from saline solutions, J. Environ. Chem. Eng., 5 (2017) 1754–1762.
[38] R. Khandanlou, M. Bin Ahmad, K. Shameli, K. Kalantari, Synthesis and characterization of rice straw/Fe_3O_4 nanocomposites by a quick precipitation method, Molecules, 18 (2013) 6597–6607.
[39] B. Kakavandi, R.R. Kalantary, A.J. Jafari, S. Nasseri, A. Ameri, A. Esrafili, A. Azari, Pb(II) adsorption onto a magnetic composite of activated carbon and superparamagnetic Fe_3O_4 nanoparticles: experimental and modeling study, CLEAN – Soil, Air, Water, 43 (2015) 1157–1166.
[40] S. Nethaji, A. Sivasamy, A.B. Mandal, Preparation and characterization of corn cob activated carbon coated with nano-sized magnetite particles for the removal of Cr(VI), Bioresour. Technol., 134 (2013) 94–100.
[41] S. Luo, M.-N. Shen, F. Wang, Q.R. Zeng, J.-H. Shao, J.-D. Gu, Synthesis of Fe_3O_4-loaded porous carbons developed from rice husk for removal of arsenate from aqueous solution, Int. J. Environ. Sci. Technol., 13 (2016) 1137–1148.
[42] P. Lodeiro, J.L. Barriada, R. Herrero, M.E. Sastre de Vicente, The marine macroalga *Cystoseira baccata* as biosorbent for cadmium(II) and lead(II) removal: kinetic and equilibrium studies, Environ. Pollut., 142 (2006) 264–273.
[43] M. Ghasemi, S. Mashhadi, J. Azimi-Amin, Fe_3O_4/AC nanocomposite as a novel nano adsorbent for effective removal of cationic dye: process optimization based on Taguchi design method, kinetics, equilibrium and thermodynamics, J. Water Environ. Nanotechnol., 3 (2018) 321–336.
[44] S. Zhang, Z. Wang, H. Chen, C. Kai, M. Jiang, Q. Wang, Z. Zhou, Polyethylenimine functionalized Fe_3O_4/steam-exploded rice straw composite as an efficient adsorbent for Cr(VI) removal, Appl. Surf. Sci., 440 (2018) 1277–1285.
[45] X. Chen, J. Yu, Z. Zhang, C. Lu, Study on structure and thermal stability properties of cellulose fibers from rice straw, Carbohydr. Polym., 85 (2011) 245–250.
[46] S.M. Yakout, Monitoring the changes of chemical properties of rice straw–derived biochars modified by different oxidizing agents and their adsorptive performance for organics, Biorem. J., 19 (2015) 171–182.
[47] A.F. Bishay, Environmental application of rice straw in energy production and potential adsorption of uranium and heavy metals, J. Radioanal. Nucl. Chem., 286 (2010) 81–89.
[48] A.R. Bagheri, M. Ghaedi, A. Asfaram, A.A. Bazrafshan, R. Jannesar, Comparative study on ultrasonic assisted adsorption of dyes from single system onto Fe_3O_4 magnetite nanoparticles loaded on activated carbon: experimental design methodology, Ultrason. Sonochem., 34 (2017) 294–304.
[49] A. Ebrahimian Pirbazari, E. Saberikhah, S.S. Habibzadeh Kozani, Fe_3O_4–wheat straw: preparation, characterization and its application for methylene blue adsorption, Water Resour. Ind., 7–8 (2014) 23–37.
[50] R. Khandanlou, M.B. Ahmad, H.R.F. Masoumi, K. Shameli, M. Basri, K. Kalantari, Rapid adsorption of copper(II) and lead(II) by rice straw/Fe_3O_4 nanocomposite: optimization, equilibrium isotherms, and adsorption kinetics study, PLoS One, 10 (2015) 1–19, doi: 10.1371/journal.pone.0120264.
[51] U.K. Sahu, S. Sahu, S.S. Mahapatra, R.K. Patel, Cigarette soot activated carbon modified with Fe_3O_4 nanoparticles as an effective adsorbent for As(III) and As(V): material preparation, characterization and adsorption mechanism study, J. Mol. Liq., 243 (2017) 395–405.
[52] J. Ruey-Shin, Y. Yao-Chung, L. Chien-Shiun, L. Kuen-Song, L. Hsi-Chuan, W. Sea-Fue, S. An-Cheng, Synthesis of magnetic Fe_3O_4/activated carbon nanocomposites with high surface area as recoverable adsorbents, J. Taiwan Inst. Chem. Eng., 90 (2018) 51–60.
[53] M. Madhava Rao, D.H.K. Kumar Reddy, P. Venkateswarlu, K. Seshaiah, Removal of mercury from aqueous solutions using activated carbon prepared from agricultural by-product/waste, J. Environ. Manage., 90 (2009) 634–643.
[54] R. Baby M.Z. Hussein, Ecofriendly approach for treatment of heavy-metal-contaminated water using activated carbon of kernel shell of oil palm, Materials (Basel), 13 (2020) 11–13.
[55] N.H. Pathode, D.V. Parwate, I. Das Sarma, Separation of Zn(II) and Cd(II) ions from synthetic waste water by adsorption on activated carbon derived from tridax procumbens, Anal. Chem. Lett., 4 (2014) 113–122.
[56] D. Kołodyńska, J. Krukowska, P. Thomas, Comparison of sorption and desorption studies of heavy metal ions from biochar and commercial active carbon, Chem. Eng. J., 307 (2017) 353–363.
[57] H. Karami, Heavy metal removal from water by magnetite nanorods, Chem. Eng. J., 219 (2013) 209–216.
[58] H. Aydin, Y. Bulut, Ç. Yerlikaya, Removal of copper(II) from aqueous solution by adsorption onto low-cost adsorbents, J. Environ. Manage., 87 (2008) 37–45.
[59] M.N. Mohamad Ibrahim, W.S. Wan Ngaha, M.S. Norliyana, W.R. Wan Daud, M. Rafatullah, O. Sulaiman, R. Hashim, A novel agricultural waste adsorbent for the removal of lead(II) ions from aqueous solutions, J. Hazard. Mater., 182 (2010) 377–385.
[60] B. D'Cruz, M. Madkour, M.O. Amin, E. Al-Hetlani, Efficient and recoverable magnetic AC-Fe_3O_4 nanocomposite for rapid removal of promazine from wastewater, Mater. Chem. Phys., 240 (2020) 122109, doi: 10.1016/j.matchemphys.2019.122109.
[61] H.A. Sani, M.B. Ahmad, M.Z. Hussein, N.A. Ibrahim, A. Musa, T.A. Saleh, Nanocomposite of ZnO with montmorillonite for removal of lead and copper ions from aqueous solutions, Process Saf. Environ. Prot., 109 (2017) 97–105.
[62] U. Garg, M.P. Kaur, G.K. Jawa, D. Sud, V.K. Garg, Removal of cadmium(II) from aqueous solutions by adsorption on agricultural waste biomass, J. Hazard. Mater., 154 (2008) 1149–1157.
[63] Y. Niu, W. Hu, M. Guo, Y. Wang, J. Jia, Z. Hu, Preparation of cotton-based fibrous adsorbents for the removal of heavy metal ions, Carbohydr. Polym., 225 (2019) 115218, doi: 10.1016/j.carbpol.2019.115218.
[64] M. Abdulkarim F.A. Al-Rub, Adsorption of lead ions from aqueous solution onto activated carbon and chemically-modified activated carbon prepared from date pits, Adsorpt. Sci. Technol., 22 (2004) 119–134.
[65] S. Qaiser, A.R. Saleemi, M. Umar, Biosorption of lead(II) and chromium(VI) on groundnut hull: equilibrium, kinetics and thermodynamics study, Electron. J. Biotechnol., 12 (2009), doi: 10.2225/vol12-issue4-fulltext-6.
[66] R. Shanmugavalli, P.S.S. Shabudeen, R. Venckatesh, K. Kadirvelu, S. Madhavakrishnan, S. Pattabhi, Uptake of Pb(II)

ion from aqueous solution using silk cotton hull carbon: an agricultural waste biomass, E-J. Chem., 3 (2006) 218–229.
[67] R. Rehman, J. Anwar, T. Mahmud, Sorptive removal of lead(II) from water using chemically modified mulch of *Madhuca longifolia* and *Polyalthia longifolia* as novel biosorbents, Desal. Water Treat., 51 (2013) 2624–2634.
[68] J.V. Milojković, M.L. Mihajlović, M.D. Stojanović, Z.R. Lopičić, M.S. Petrović, T.D. Šoštarić, M.Đ. Ristić, Pb(II) removal from aqueous solution by *Myriophyllum spicatum* and its compost: equilibrium, kinetic and thermodynamic study, J. Chem. Technol. Biotechnol., 89 (2014) 662–670.
[69] M.N. Sahmoune, Evaluation of thermodynamic parameters for adsorption of heavy metals by green adsorbents, Environ. Chem. Lett., 17 (2019) 697–704.
[70] M. Rahimizadeh, A. Liaghat, Biosorbents for adsorption of heavy metals: a review, Int. Conf. Environ. Sci. Eng. Technol. (CESET 2015), 5 (2015) 1–13.
[71] R. Ayyappan, A.C. Sophia, K. Swaminathan, S. Sandhya, Removal of Pb(II) from aqueous solution using carbon derived from agricultural wastes, Process Biochem., 40 (2005) 1293–1299.
[72] M. Chaudburi, S.R.M. Kutty, S.H. Yusop, Copper and cadmium adsorption by activated carbon prepared from coconut coir, Nat. Environ. Pollut. Technol., 9 (2010) 25–28.
[73] F.M.S.E. El-Dais, A.E.O. Sayed, B.A. Salah, M.E.H. Shalabi, Removal of nickel(II) from aqueous solution via carbonized date pits and carbonized rice husks, Eurasian Chem. J., 13 (2011) 267–277.
[74] P.C. Mishra, R.K. Patel, Removal of lead and zinc ions from water by low cost adsorbents, J. Hazard. Mater., 168 (2009) 319–325.
[75] B.M.W.P.K. Amarasinghe, R.A. Williams, Tea waste as a low cost adsorbent for the removal of Cu and Pb from wastewater, Chem. Eng. J., 132 (2007) 299–309.
[76] D. Mohan, H. Kumar, A. Sarswat, M. Alexandre-Franco, C.U. Pittman, Cadmium and lead remediation using magnetic oak wood and oak bark fast pyrolysis bio-chars, Chem. Eng. J., 236 (2014) 513–528.
[77] H. Ravishankar, J. Wang, L. Shu, V. Jegatheesan, Removal of Pb(II) ions using polymer based graphene oxide magnetic nano-sorbent, Process Saf. Environ. Prot., 104 (2016) 472–480.
[78] F.M.S.E. El-Dars, M.A.G. Elngar, S.T. Abdel-Rahim, N.A. El-Hussiny, M.E.H. Shalabi, Kinetic of nickel(II) removal from aqueous solution using different particle size of water – cooled blast furnace slag, Desal. Water Treat., 54 (2015) 769–778.
[79] B. Belhamdi, Z. Merzougui, M. Trari, A. Addoun, A kinetic, equilibrium and thermodynamic study of L-phenylalanine adsorption using activated carbon based on agricultural waste (date stones), J. Appl. Res. Technol., 14 (2016) 354–366.
[80] M.H. Ali, A.E.M. Hussian, A.M. Abdel-Satar, M.E. Goher, A. Napiórkowska-Krzebietke, A.M. Abd El-Monem, The isotherm and kinetic studies of the biosorption of heavy metals by non-living cells of chlorella vulgaris, J. Elem., 21 (2016) 1263–1276.
[81] I. Lestari, E. Kurniawan, D.R. Gusti, Yusnelti, Magnetite Fe_3O_4-activated carbon composite as adsorbent of rhodamine B dye, IOP Conf. Ser.: Earth Environ. Sci., 483 (2020), doi: 10.1088/1755-1315/483/1/012046.
[82] N.N. Nassar, Kinetics, equilibrium and thermodynamic studies on the adsorptive removal of nickel, cadmium and cobalt from wastewater by superparamagnetic iron oxide nanoadsorbents, Can. J. Chem. Eng., 90 (2012) 1231–1238.
[83] S.S. Banerjee, D.H. Chen, Fast removal of copper ions by gum arabic modified magnetic nano-adsorbent, J. Hazard. Mater., 147 (2007) 792–799.
[84] N. Kataria, V.K. Garg, Green synthesis of Fe_3O_4 nanoparticles loaded sawdust carbon for cadmium(II) removal from water: regeneration and mechanism, Chemosphere, 208 (2018) 818–828.
[85] Y. Li, S. Zhu, Q. Liu, Z. Chen, J. Gu, C. Zhu, T. Lu, D. Zhang, J. Ma, N-doped porous carbon with magnetic particles formed in situ for enhanced Cr(VI) removal, Water Res., 47 (2013) 4188–4197.
[86] G. López-Téllez, C.E. Barrera-Díaz, P. Balderas-Hernández, G. Roa-Morales, B. Bilyeu, Removal of hexavalent chromium in aquatic solutions by iron nanoparticles embedded in orange peel pith, Chem. Eng. J., 173 (2011) 480–485.